RUSSIAN JOURNAL OF EARTH SCIENCES, VOL. 4, NO. 1, PAGES 1–17, FEBRUARY 2002

Global stresses in the Western Europe lithosphere and the collision forces in the Africa-Eurasia convergence zone

Sh. A. Mukhamediev

Schmidt United Institute of Physics of the Earth, Russian Academy of Sciences

Abstract. The experimentally determined directions of the maximum horizontal compressive stress $S_{\mathrm{H,max}}$ in the western European stress province (WESP) of the West European platform are mostly oriented northwest with an average azimuth of $325^\circ \pm 26^\circ$. The traditional approach to the mathematical modeling of the stress field in the Western Europe lithosphere (as well as in other stable lithospheric blocks) is based on an elastic model of the medium and boundary conditions that specify stresses and/or displacements at the entire perimeter of the region studied. In the particular case of Western Europe, poorly constrained boundary conditions should be set at the southern (in the collision zone of the African and Eurasian plates) and eastern boundaries of the region. For this purpose, experimental directions of $S_{\mathrm{H,max}}$ are used as constraints on the sought-for solution. However, even if the experimental directions of $S_{\mathrm{H,max}}$ agree well with their theoretical estimates, model stress magnitudes are still sensitive to the choice of model boundary conditions.A basically different approach proposed and implemented in this work for determining the field of tectonic stresses uses the experimental directions of $S_{\mathrm{H,max}}$ as input information rather than constraints on the sought-for solution. The spatially persisting strike of the $S_{\mathrm{H,max}}$ axis makes it possible to construct the field of straight trajectories of principal stresses on the WESP territory. The problem of stress determination is then reduced to the hyperbolic-type problem of integrating the equilibrium equations that does not require postulating constitutive relations, and the boundary conditions are only specified on some part of the boundary of the model region. The lithosphere material can be mechanically anisotropic and inhomogeneous. Stresses $\mathbf{t}^{\mathrm{R}}$ produced by the ridge push were specified in this work on a segment of the Mid-Atlantic Ridge, and stresses $\mathbf{t}^{\mathrm{C}}$ due to the Africa-Europe collision were specified in the convergence zone. No boundary conditions are required at the eastern boundary of the region studied. Supposedly, straight trajectories of stresses can be extended into oceanic lithosphere areas adjacent to the continent. The formulation of the problem presented in the paper provides substantial constraints on the collision stresses $\mathbf{t}^{\mathrm{C}}$. These constraints directly result from the equilibrium conditions of the Western Europe lithosphere rather than from the plate convergence kinematics in the collision zone. A simple analytical expression obtained for the tensor of global tectonic stresses in the study region indicates that the $S_{\mathrm{H,max}}$ magnitude decreases in the NW direction. The minimum horizontal stress in the WESP region is shown to be sensitive to the direction of the collision stresses $\mathbf{t}^{\mathrm{C}}$. This stress whose modulus increases in the SE direction is compressive, zero or tensile depending on whether the vector of collision stresses $\mathbf{t}^{\mathrm{C}}$ deviates westward from the $S_{\mathrm{H,max}}$ direction, coincide with it or deviates eastward from it. The modification of the inferred solution incorporating stresses applied at the base of the lithospheric plate is discussed.

Paper number TJE02083.
ISSN: 1681–1208 (online)

The online version of this paper was published 8 March 2002.
URL: http://rjes.agu.org/v04/tje02083/tje02083.htm

Introduction

A large amount of experimental data on *in situ* stresses has been gathered over a nearly half-century period of studying the stress state of the Western Europe lithosphere. The experimental data on the present tectonic stresses were ob-

tained from both instrumental measurements and the analysis of seismological observations. Even the early measurements of stresses made in the 1960s and early 1970s (e.g. see [*Ahorner,* 1975; *Greiner,* 1975]) revealed a uniform NW orientation of the axis of the maximum horizontal compressive stress $S_{\mathrm{H,max}}$ and provided some constraints on the tectonics and seismicity of large geological structures such as the Rhine system of grabens [*Ahorner,* 1975; *Illies and Greiner,* 1979; and others]. Later, new constraints on stresses were gained and the existing data were generalized as a result of investigations within the framework of the World Stress Map (WSM) Project [*Grünthal and Stromeyer,* 1992; *Müller et al.,* 1992; *Zoback,* 1992; *Zoback et al.,* 1989]. In particular, these studies confirmed that the $S_{\mathrm{H,max}}$ axis distribution is homogeneous over large areas in Western Europe, demonstrated that the $S_{\mathrm{H,max}}$ direction is virtually independent of depth and determined the variation of the $S_{\mathrm{H,max}}$ orientation pattern in the direction toward the East European platform. Large geological structures in Western Europe such as the Alps were shown to disturb the homogeneity of the global stress orientation on regional and local scales.[1]

Later studies were focused on the verification and improvement of stress data and on gaining new results for Western Europe regions and structures. New measurements of present stresses were made in Northern Europe (Barents and North seas) [*Gölke and Brudy,* 1996; *Wirput and Zoback,* 2000], on the Iberian Peninsula (where paleostresses were also analyzed) [*Andeweg et al.,* 1999; *De Vicente et al.,* 1996], in British Isles [*Becker and Davenport,* 2001], in the Apennines [*Frepoli and Amato,* 2000; *Montone et al.,* 1999], and in France, Germany and Austria [*Cornet and Yin,* 1995; *Delouis et al.,* 1993; *Plenefisch and Bonjer,* 1997; *Reinecker and Lenhardt,* 1999; *Scotti and Cornet,* 1994; *Yin and Cornet,* 1994]. Tectonic stresses of second order were studied and their geodynamic interpretations were proposed for the Alps [*Delouis et al.,* 1993; *Eva and Solarino,* 1998; *Eva et al.,* 1998; *Regenauer-Lieb,* 1996], Apennines [*Boncio and Lavecchia,* 2000; *Collettini et al.,* 2000], and Rhinegraben [*Delouis et al.,* 1993; *Plenefisch and Bonjer,* 1997].

It is assumed that the global stress field in Western Europe is mainly controlled by the push from the central and northern segments of the Mid-Atlantic Ridge (MAR) and by the collision forces arising due to convergence of Africa and Europe [*Grünthal and Stromeyer,* 1992; *Müller et al.,* 1992]. As distinct from the push force, both the modulus and direction of collision forces have been poorly studied [*Albarello et al.,* 1995; *Gölke and Coblenz,* 1996; *Richardson,* 1992]. Also ambiguous are geological-geophysical kinematic models [*Albarello et al.,* 1995; *Argus et al.,* 1989; *Savostin et al.,* 1986] and satellite geodesy data on movements and deformations in the collision zone [*Campbell and Nothnagel,* 2000; *Noomen et al.,* 1996].

In this context, results of numerical modeling of the stress field in Western Europe based on the traditional approach that requires the specification of boundary conditions on the entire boundary of the study region (e.g. see [*Gölke and Coblenz,* 1996]) are very sensitive to the assumptions on the characteristics of collision forces and on the poorly constrained stresses (or displacements) at the eastern boundary. The coincidence of theoretical and experimental directions of $S_{\mathrm{H,max}}$ at the stress measurement points within the study area by no means remove the ambiguity of resulting solutions [*Mukhamediev,* 2000; *Mukhamediev and Galybin,* 2001].

The approach applied in this work to the mathematical modeling of the tectonic stress field was proposed in [*Mukhamediev,* 1991]. The problem is reduced to the construction of the field of principal stress trajectories and the subsequent integration of equilibrium equations, with boundary conditions specified only on part of the Western Europe boundary. In principle, this approach allows one to impose significant constraints on the distribution pattern of forces arising due to the Africa-Europe convergence.

1. Experimental Data on the Tectonic Stresses in the Western Europe Lithosphere and Convergence Kinematics of Africa and Eurasia

1.1. Methods of Stress Measurements

The following methods were used for local instrumental measurements of stresses in Western Europe:

– various overcoring methods applied to unload samples taken during drilling operations in mines, tunnels and quarries [*Becker and Davenport,* 2001; *Greiner,* 1975; *Greiner and Illies,* 1977; *Illies and Greiner,* 1979; and others];

– jacking methods according to which a plane or circular slot is cut in a rock mass, and a loading device (jack) inserted into the slot raises pressure until the strain developed during the creation of the slot vanishes [*Froidevaux et al.,* 1980];

– borehole slotting methods for measuring the strain release near slots cut in borehole walls [*Amadei and Stephanson,* 1997; *Becker,* 1999];

– methods of hydraulic fracturing which determine both the direction of extreme horizontal stresses and the minor principal stress magnitude [*Amadei and Stephanson,* 1997; *Zoback et al.,* 1993];

– borehole caliper measurements for detecting ellipticity caused by borehole breakouts [*Gölke and Brudy,* 1996; *Wirput and Zoback,* 2000; *Zoback et al.,* 1989].

Methods of reconstructing the present stress state of the Western Europe lithosphere from seismological data have recently become widespread [*De Vicente et al.,* 1996; *Frepoli and Amato,* 2000; *Eva and Solarino,* 1998; *Eva et al.,* 1998; *Montone et al.,* 1999; *Plenefisch and Bonjer,* 1997; *Scotti and Cornet,* 1994]. Some authors associate the directions of extreme stresses with the axes P and T of focal mechanisms (e.g. see [*Ahorner,* 1975; *Montone et al.,* 1999]). Presently, the principal axis orientations of the stress tensor $\mathbf{T}$ are mostly determined from a certain set of focal mechanisms of earthquakes using methods developed in [*Gephart and Forthsyth,* 1984; *Rivera and Cisternas,* 1990; and others].

[1]Global stresses are understood here as stresses transmitted from lithospheric plate boundaries in accordance with the term "stresses of first order" introduced by *Zoback* [1992]. In this context, regional and local disturbances are induced by "stresses of second order" [*Zoback,* 1992].

These methods are based on the assumption that the slip direction and the direction of the maximum resolved shear stress coincide on the fault slip planes and, in the opinion of their authors, allow the reconstruction of the principal axis directions and the parameter R characterizing the relative differences of principal stresses.[2]

Theoretical substantiation of some of the aforementioned methods is based on several restrictive assumptions on rock properties and the stress distribution patterns in rock masses where stresses were measured. The presence of large stress gradients, local heterogeneities in samples and rocks masses, departures of rocks from linear-elastic behavior and other factors can be sources of significant errors in interpretation of the measurements [*Grob et al.,* 1975; *Harper and Szymanski,* 1991; *Ranalli,* 1975; *Rutqvist et al.,* 2000]. Some authors combine various methods in order to more reliably determine local stress state elements. Thus, an algorithm of joint inversion of seismological and hydraulic fracturing data was applied to the stress determination in central France [*Cornet and Yin,* 1995; *Yin and Cornet,* 1994], and constraints on the stress state in the overdeep KTB borehole area (southern Germany) were gained from both hydraulic fracturing results and caliper measurements [*Zoback et al.,* 1993].

Various methods differ in the amount of information on stress state elements that they can provide. The overcoring methods alone can, in principle, provide constraints on all components of the local stress tensor **T**. Other methods can be helpful for determining the principal axis orientations of the tensor **T** and, perhaps, for gaining additional constraints on the local stress state. However, the overcoring methods are affective only at small depths because, similar to the jacking methods, they are applied near the Earth's surface. The hydraulic fracturing methods and borehole caliper measurements are sources of data on stresses at depths of up to a few kilometers and fill the gap between near-surface indicators on the one hand and seismological data on the other [*Amadei and Stephanson,* 1997]. Focal mechanisms of earthquakes are actually the only source of information about stresses in Western Europe at depths greater than 5 km [*Müller et al.,* 1992].

Experimental measurements usually indicate that two of the three principal axes of the stress tensor **T** are subhorizontal [*Müller et al.,* 1997; *Zoback,* 1992; *Zoback et al.,* 1989; and others].[3] This observation makes it possible to introduce the notion of the stress regime. The stress regimes can be classified as those of compression ($S_{\mathrm{H,max}} > S_{\mathrm{H,min}} > S_{\mathrm{V}}$), shear ($S_{\mathrm{H,max}} > S_{\mathrm{V}} > S_{\mathrm{H,min}}$) and extension ($S_{\mathrm{V}} > S_{\mathrm{H,max}} > S_{\mathrm{H,min}}$) [*Zoback et al.,* 1989]. Henceforward, compressive stresses are positive; $S_{\mathrm{H,max}}$ and $S_{\mathrm{H,min}}$ are, respectively, maximum and minimum normal horizontal stresses; and S_{V} is the principal vertical stress due to the weight of rocks. After to *Anderson* [1951], the aforementioned regimes are often interpreted in terms of faulting deformations and are referred to as, respectively, regimes of thrust or reverse faulting, strike-slip faulting and normal faulting [*Amadei and Stephanson,* 1997; *Zoback et al.,* 1989].

In addition to the present-day *in situ* stresses, paleostresses were determined in various regions of Western Europe. These determinations are based on such methods as the analysis of tectonic stilolites [*Illies,* 1975; *Letouzev,* 1986], inversion of striation data from variously oriented planes of joints in rocks [*Letouzev,* 1986] and faulting data from variously oriented faults [*De Vicente et al.,* 1996], and examination of the attitude, strike and deformation of geological bodies [*Andeweg et al.,* 1999]. The difficulties of dating the activity periods of paleostresses were in part compensated for by the fact that their kinematic indicators were studied in relatively young rocks (usually not older than the Late Cretaceous).

1.2. Stress Orientations and Deformation Regimes in the Western Europe Lithosphere

Experimental data indicate that, similar to some other regions of the Earth, the Western Europe lithosphere is commonly subjected to the action of the stress $S_{\mathrm{H,max}}$ uniformly oriented northwest and north-northwest (Figure 1). These results obtained in the 1960s and early 1970s (e.g. see [*Ahorner,* 1975; *Greiner,* 1975]) were generalized within the framework of the WSM Project [*Grünthal and Stromeyer,* 1992; *Müller et al.,* 1992; *Zoback,* 1992; *Zoback et al.,* 1989; and others]. The NW orientation of $S_{\mathrm{H,max}}$ cease to be predominant east of ≈14°E [*Grünthal and Stromeyer,* 1992; *Müller et al.,* 1992]. The $S_{\mathrm{H,max}}$ direction is virtually independent of depth and is not affected by short-wavelength variations in the thickness of the lithosphere, its structural features and topography [*Müller et al.,* 1992; *Richardson,* 1992]. Large geological structures (e.g. the Alps) superimpose regional signatures on the global orientation of the stresses [*Müller et al.,* 1992].

Figure 1 shows generalized directions of $S_{\mathrm{H,max}}$ inferred in [*Balling and Bauda,* 1992; *Müller et al.,* 1992]. The data generalization allows one to exclude from the analysis local disturbances in the stress orientation and to analyze the averaged regional field of the $S_{\mathrm{H,max}}$ directions as a function of driving forces applied at plate boundaries. Three large provinces of stresses have been distinguished in the spatial distribution of the $S_{\mathrm{H,max}}$ orientation in Western Europe [*Müller et al.,* 1992, 1997]:

(1) western European stress province (WESP) north of the Alps and Pyrenees, with the $S_{\mathrm{H,max}}$ axis consistently striking 325°±26° [*Ahorner,* 1975; *Grünthal and Stromeyer,* 1992; *Illies and Greiner,* 1979; *Müller et al.,* 1992, 1997; *Zoback,* 1992; *Zoback et al.,* 1989];

(2) northern European stress province north of ≈55°N including Fennoscandia and characterized by a wide scatter in the azimuths of the $S_{\mathrm{H,max}}$ axis strike (300°±45°) [*Gölke and Brudy,* 1996; *Müller et al.,* 1992; *Wirput and Zoback,* 2000; and others];

(3) Aegean-Anatolian stress province approximately defined by the coordinates (27°–37°E, 34°–42°N) and characterized by an E-W orientation of the $S_{\mathrm{H,max}}$ axis (265°±27°), with the normal and strike-slip faulting regimes prevailing

[2]Various aspects of these methods were criticized (e.g. see [*Gapais et al.,* 2000; *Mukhamediev,* 1993; *Twiss and Unrun,* 1998]).

[3]Some methods (e.g. stress determinations from breakouts in vertical boreholes) postulate that two principal axes of the stress tensor **T** are horizontal.

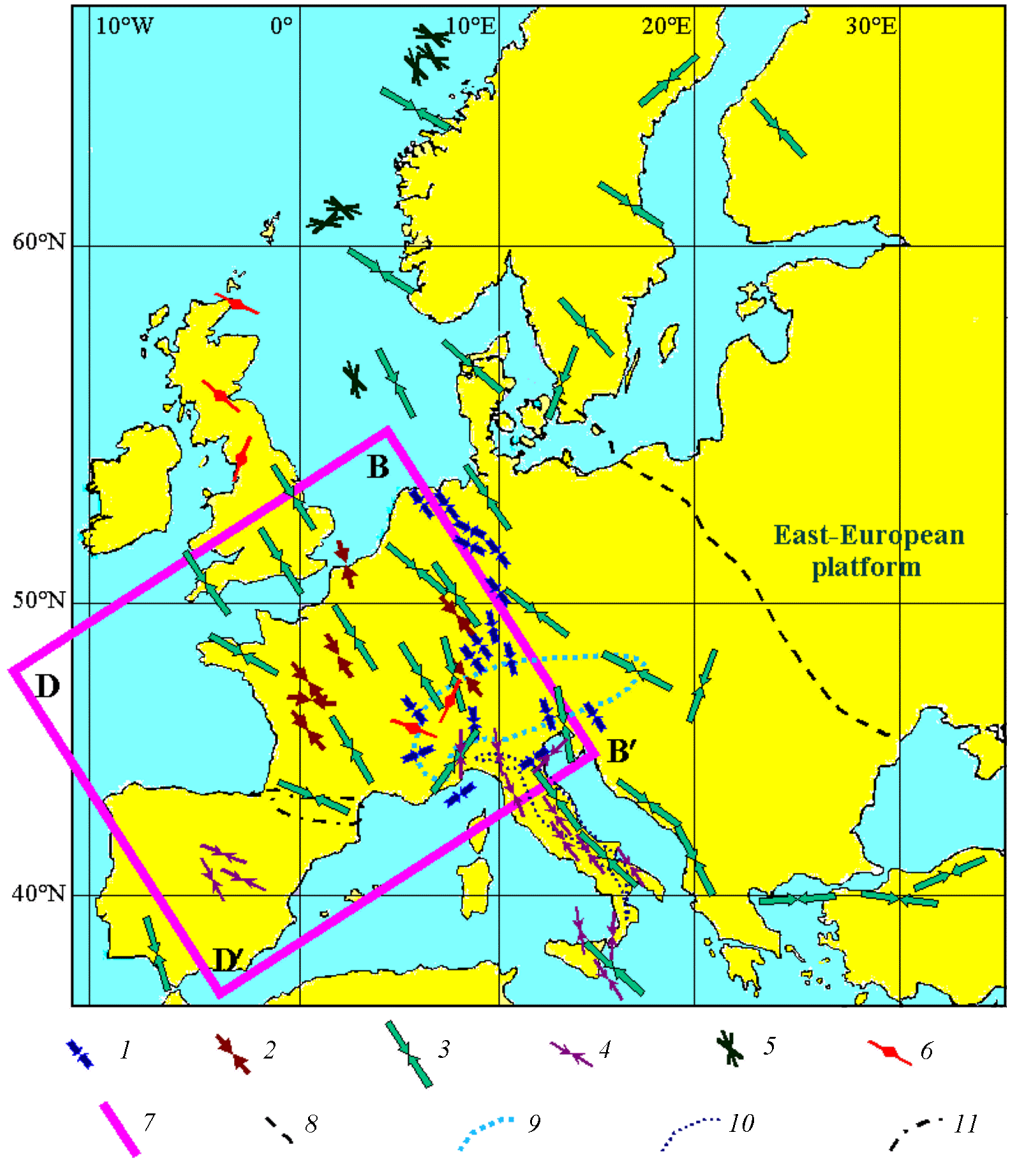

Figure 1. Experimentally determined directions of the present maximum compressive stress $S_{\mathrm{H,max}}$ in the Western Europe lithosphere: (1) the $S_{\mathrm{H,max}}$ directions determined from instrumental and seismological observations in the late 1960s-early 1970s (after [*Ahorner,* 1975]); (2) the $S_{\mathrm{H,max}}$ directions determined in Germany and France from instrumental (overcoring and flat jack) measurements [*Froidevaux et al.,* 1980; *Greiner,* 1975]; (3) averaged $S_{\mathrm{H,max}}$ directions determined from various stress indicators and compiled from WSM data [*Balling and Bauda,* 1992; *Müller et al.,* 1992]; (4) generalized $S_{\mathrm{H,max}}$ directions obtained from seismological observations in Spain [*De Vicente et al.,* 1996] and from data on borehole breakouts and focal mechanisms in Italy [*Montone et al.,* 1999]; (5) generalized $S_{\mathrm{H,max}}$ directions obtained from data on borehole breakouts in the North Sea [*Gölke and Brudy,* 1996; *Wirput and Zoback,* 2000]; (6) averaged $S_{\mathrm{H,max}}$ directions determined from overcoring data in British Isles [*Becker and Davenport,* 2001] and from borehole slotting data in the Swiss Alps [*Becker,* 1999]; (7) WESP boundary accepted in the present work; (8) Tornquist-Teisseyre line (western boundary of the East European platform); (9)–(11) boundaries of the (9) Alps, (10) Apennines and (11) Pyrenees.

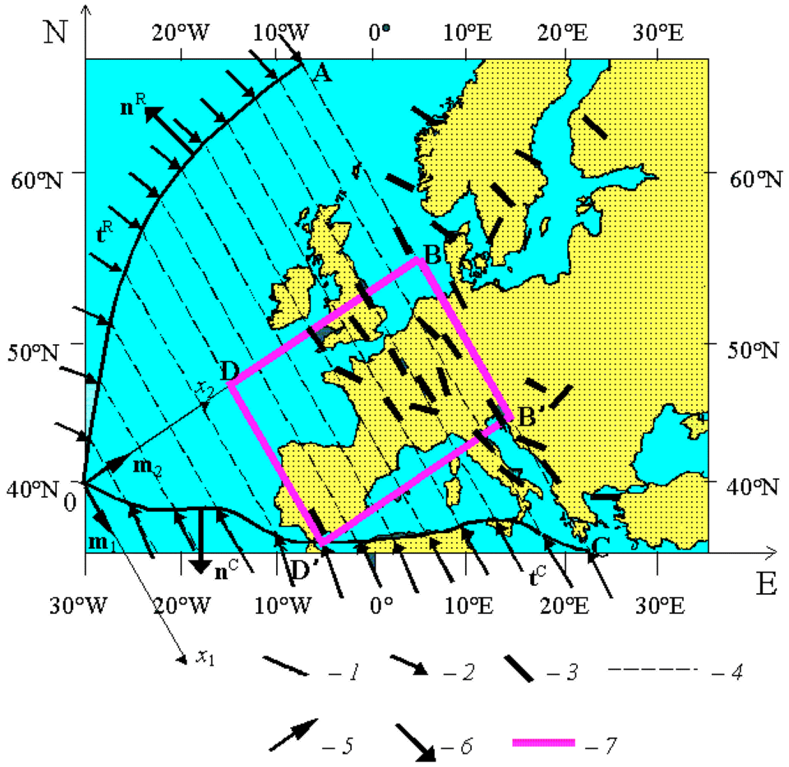

Figure 2. Geometry of the study region, averaged directions of the horizontal stress $S_{\mathrm{H,max}}$ [*Balling and Bauda,* 1992; *Müller et al.,* 1992] and the approximate field of its straight trajectories: (1) plate boundaries ($0A$ is the generalized trajectory of the MAR segment and $0B$ is the boundary segment between the African and Eurasian plates); (2) boundary stress vectors; (3) experimentally determined directions of $S_{\mathrm{H,max}}$; (4) approximate trajectories of $S_{\mathrm{H,max}}$; (5) unit vectors of principal axes of the model stress tensor $\mathbf{T}$; (6) unit vectors normal to the boundary of the region; (7) WESP boundary accepted in this work.

west and east of ≈30°E, respectively [*Gölke and Coblenz,* 1996; *Müller et al.,* 1992, 1997; *Zoback et al.,* 1989].

The aforementioned generalized properties of the stress field in various regions and large geological structures of Western Europe were confirmed and, in some cases, significantly revised by later investigations. In the context of this work, most interesting is the WESP region distinguished by the most uniform distribution of principal stresses. The WESP territory is dominated by the strike-slip faulting regime with nearly vertical orientation of the intermediate principal stress, although WESP also includes regions dominated by extension and compression regimes [*Müller et al.,* 1992, 1997]. The boundaries between the large provinces of stresses mentioned above can be delineated only tentatively; therefore, the WESP territory adopted here (the rectangle $BB'D'D$ in Figures 1 and 2) is somewhat larger than the territory considered in [*Müller et al.,* 1992, 1997]. I discuss in more detail the spatial distribution of the stress state characteristics in WESP and adjacent regions.

The uniform NW orientation of the maximum horizontal compressive stress of first order is well expressed on the most territory of France, as is indicated by instrumental and seismological observations [*Cornet and Yin,* 1995; *Delouis et al.,* 1993; *Froidevaux et al.,* 1980; *Scotti and Cornet,* 1994; *Yin and Cornet,* 1994]. The same orientation is typical of British Isles (e.g. see [*Becker and Davenport,* 2001]). The NW orientation of the $S_{\mathrm{H,max}}$ axis in Germany and Belgium is supported by both instrumental measurements [*Greiner,* 1975] and seismicity pattern in linear weakened zones; focal mechanisms indicate the strike-slip faulting regime in such of these zones that strike in the NNE and WNW directions (the Upper Rhinegraben, Belgian zone, and others), i.e. roughly along the direction of the maximum horizontal shear stress $\tau_{\max}$, whereas the extension regime characterizes, for example, the Lower Rhinegraben striking NW (i.e. along the $S_{\mathrm{H,max}}$ direction), as is evident from normal motions on fault planes parallel to the graben strike [*Ahorner,* 1975; *Delouis et al.,* 1993; *Illies and Greiner,* 1979; *Plenefisch and Bonjer,* 1997]. Reliable fault plane solutions for earthquakes in the western Pyrenees also indicate the NNW and NW orientations of the $S_{\mathrm{H,max}}$ axis [*Delouis et al.,* 1993]. The convergence of Africa and Europe gave rise to the formation of sedimentary basins in central Spain, which advantageous for the reconstruction of the neotectonic paleostress evolution [*Andeweg et al.,* 1999; *De Vicente et al.,* 1996]. Paleostress studies and the analysis of focal mechanisms showed

that, from the Middle Miocene to the present time, $S_{H,max}$ axis azimuths have remained within a 310°–340° interval [*De Vicente et al.,* 1996].

The present pattern of stress orientations is most distorted in seismically active regions of the Apennines and Alps. Strong variations in stress orientations over comparatively small distances superimposed on the global field in the Apennines are due to the underthrusting of the Adriatic microplate beneath the southern Alps and other complex geodynamic processes developing in the immediate vicinity of this region [*Frepoli and Amato,* 2000; *Montone et al.,* 1999]. However, the extension regime prevailing over the most territory of northern and central Italy, the orientations of principal stress axes retain the same properties as in the WESP province, namely: the $S_{H,min}$ axis has the NE orientation (orthogonal to the Apennines strike) [*Frepoli and Amato,* 2000; *Montone et al.,* 1999]. Tensile deformations result in thinning of the crust (20–25 km) and higher heat flow values [*Collettini et al.,* 2000]. Structural features associated with the NE orientation of the $S_{H,min}$ axis are large, NW-NNW striking active normal faults accounting for the main seismicity and Pliocene-Quaternary sedimentary basins elongated in the same direction [*Boncio and Lavecchia,* 2000; *Collettini et al.,* 2000]. The compression regime with the NE striking $S_{H,max}$ axis exists only in a small area in the east of northern Apennines (near the Adriatic coast) [*Collettini et al.,* 2000; *Frepoli and Amato,* 2000; *Montone et al.,* 1999].

The compression axes in the Alps, as constrained by focal mechanisms of earthquakes, are on a first approximation close to the directions of horizontal shortening of the crust reconstructed from the kinematic analysis of neotectonic structures [*Balling and Bauda,* 1992; *Müller et al.,* 1992]. The maximum horizontal stress axis trends nearly N-S in the Swiss Alps, as is also established from data of instrumental measurements [*Becker,* 1999]. The properties of the stress field mentioned above are evidence that the deformation pattern in this region has not changed over a few last millions of years. Later and more detailed studies of seismicity discovered an inhomogeneous fine structure of the stress axes distribution [*Eva and Solarino,* 1998; *Eva et al.,* 1998]. Thus, the observed spatial variations in the stress regime yield evidence of a near-surface extension regime superimposed on the regional compression regime. This effect is accounted for by gravitational spreading at ridge crests [*Eva and Solarino,* 1998]. Significant lateral inhomogeneity of the stress field in the southwestern Alps is related to an arcuate geometry of the ridges [*Delouis et al.,* 1993]. Other interpretations of the stress field pattern in the Alps in terms of regional geodynamic models are also known. Thus, *Regenauer-Lieb* [1996] interprets the stress-strain state in the region within the framework of a model in which a relatively rigid "Italian-Adriatic die" is indented in the NW direction into the Western Europe lithosphere.

The overview of experimental data on the stress orientations suggests a nearly uniform global NW orientation of the $S_{H,max}$ axis in the Western Europe lithosphere. Regional disturbances in the field of trajectories mainly arise as a response of structural and mechanical inhomogeneities of the lithosphere to the aforementioned global compression direction. The majority of researchers associate the global NW orientation of the compression axis with driving forces: the push produced by MAR and the collision force due to the convergence of Africa and Europe. However, there is no agreement with regard to the relative contributions of these forces. It is generally supposed that the both forces are equally responsible for the observed features of the global stress field (e.g. see [*Ahorner,* 1975; *Grünthal and Stromeyer,* 1992; *Müller et al.,* 1992, 1997]). However, some authors believe that the WESP stress field can be accounted for by the push alone, without invoking the collision forces [*Gölke and Coblenz,* 1996; *Richardson,* 1992], whereas others apply only the collision forces [*Letouzev,* 1986].

1.3. Kinematics of the Africa-Europe Convergence

The kinematics of the Africa-Europe convergence was analyzed by reconstructing the motions of these plates relative to North America from magnetic lineations in northern and central Atlantic, transform fault strikes and other geological and geophysical evidence (e.g. see [*Argus et al.,* 1989; *DeMets et al.,* 1990; *Savostin et al.,* 1986]). The paleoreconstructions showed that, in the central Mediterranean, Africa and Eurasia converged in the NW-SE or N-S directions over the last 9–10 Myr [*Savostin et al.,* 1986]. The geological-geophysical reconstruction of recent movements of lithospheric plates is consistent with such a direction of convergence. The convergence occurs at a rate of 4–7 mm/yr and is accompanied by a counterclockwise rotation of Africa relative to Eurasia around a (21°N, 21°W) pole [*Argus et al.,* 1989; *DeMets et al.,* 1990; *Gripp and Gordon,* 1990]. However, these results cannot be acknowledged being unambiguous because they are based on some restrictive assumptions. In particular, plate deformations in the collision zone are neglected (whereas Africa and Eurasia converge within a fairly wide zone of active deformations), and the entire Eurasian plate is supposed to move as a rigid block. Removal of some of these assumptions can dramatically change the results of kinematic reconstructions. Thus, if the western end of Eurasia (the so-called Iberian block) is let to move independently of the rest of the Eurasian plate, the analysis of kinematic indicators in North Atlantic admits alternative solutions, namely: an NNE-SSW or NE-SW direction of the Africa-Eurasia convergence is consistent with kinematic evidence within experimental uncertainties [*Albarello et al.,* 1995].

Direct measurement of velocities in the collision zone of the African and Eurasian plates is presently based on satellite geodesy data. Very long-base interferometry (VLBI) methods [*Campbell and Nothnagel,* 2000], GPS measurements and satellite laser ranging (SLR) [*Kahle et al.,* 1998; *Noomen et al.,* 1996] are used. Unfortunately, GPS stations and SLR measurements are few in the western and central Mediterranean regions, which are of interest here, and the results of velocity measurements are much less liable to interpretation than, for example, similar measurements in the eastern Mediterranean [*Kahle et al.,* 1998; *Noomen et al.,* 1996]. The velocity vectors supporting the geological-geophysical NUVEL-1 model of plate motion [*DeMets et al.,* 1990; *Gripp and Gordon,* 1990] are obtained only at two stations in North Africa and at one station in southern Italy.

Results inconsistent with NUVEL-1 are interpreted in terms of either their statistical insignificance or local deformation processes [*Noomen et al.,* 1996]. VLBI measurements of velocity with the use of radio telescopes are also too few for their reliable interpretation. Three sites in Italy are established to move approximately in northward and northeastward directions at a rate of 3–5 mm/yr, which is treated as a response to the subduction of the African plate, whereas measurements at one site in Spain are treated as evidence for virtual immobility of the Iberian Peninsula relative to central Europe (as distinct from movements in the geological past) [*Campbell and Nothnagel,* 2000]. Velocity vectors obtained from GPS and SLR measurements poorly agree with VLBI constraints.

Note that, even if the Africa-Europe convergence kinematics is reliably reconstructed, this does not eliminate ambiguity in the determination of collision forces, which requires the knowledge of friction characteristics at the edges of interacting plates, rheological properties of rocks in the collision zone, etc. In this context, the existing conclusions concerning the amount of collision force effect on the stress state of the Western Europe lithosphere appear to be insufficiently substantiated and any steps decreasing the arbitrariness in estimates of these forces are beneficial. Without a more accurate determination of collision forces, the discussion about relative contributions of driving forces to the development of the stress field in Western Europe (see paragraph 1.2) remains, in essence, pointless. This work provides significant constraints on collision forces without invoking kinematic characteristics of the Africa-Europe convergence. Provided that the $S_{\mathrm{H,max}}$ stress direction is known in the region, these constraints are obtained from the equilibrium conditions of the Western Europe lithosphere.

2. Formulation of the Problem

The nearly horizontal orientation of two from the three principal axes of the stress tensor $\mathbf{T}$, mentioned in paragraph 1.1, admits the formulation of a 2-D problem for modeling the tectonic stresses in Western Europe. I propose a basically new approach to the solution of the problem in which experimentally determined directions of $S_{\mathrm{H,max}}$ are used as input information rather than restraints on the sought-for solution.

The region $0ABC$ in which the problem is stated includes the WESP province (Figure 2) and is bounded by MAR (its smoothed segment is shown as the curve $0A$ in Figure 2) to the west and by a boundary segment between the African and Eurasian plates (curve $0C$ in Figure 2) to the south. The southern boundary $0C$ coincides with that used in [*Gölke and Coblenz,* 1996].

Like some other authors [*Ahorner,* 1975; *Grünthal and Stromeyer,* 1992; *Müller et al.,* 1992, 1997], I assume that the sought-for 2-D field of tectonic stresses in Western Europe is due to two forces: the push from MAR and the collision force applied at the southern boundary and produced by the convergence of Africa and Europe. These forces are modeled as stress vectors $\mathbf{t}^{\mathrm{R}}$ and $\mathbf{t}^{\mathrm{C}}$ distributed, respectively, on the curves $0A$ and $0C$ (Figure 2).[4] It is reasonable to assume that the modulus $\left|\mathbf{t}^{\mathrm{R}}\right| = p^{\mathrm{R}}$ is constant along the MAR axis [*Parsons and Richter,* 1980; *Richardson,* 1992]. Let $\mathbf{k}^{\mathrm{R}}$ and $\mathbf{k}^{\mathrm{C}}$ be the directing unit vectors of $\mathbf{t}^{\mathrm{R}}$ and $\mathbf{t}^{\mathrm{C}}$, and let p^{C} be the value of the collision stresses; then

$$\mathbf{t}^{\mathrm{R}} = p^{\mathrm{R}}\mathbf{k}^{\mathrm{R}},\ \mathbf{t}^{\mathrm{C}} = p^{\mathrm{C}}\mathbf{k}^{\mathrm{C}},\ \left|\mathbf{k}^{\mathrm{R}}\right| = 1,\ \left|\mathbf{k}^{\mathrm{C}}\right| = 1,$$
$$(p^{\mathrm{R}} = \mathrm{const} > 0,\ p^{\mathrm{C}} > 0)\ . \tag{1}$$

The horizontal vectors $\mathbf{t}^{\mathrm{R}}$ and $\mathbf{t}^{\mathrm{C}}$ are directed inside the study region, producing normal stresses at the western and southern boundaries, so that

$$\mathbf{k}^{\mathrm{R}} \bullet \mathbf{n}^{\mathrm{R}} < 0, \quad \mathbf{k}^{\mathrm{C}} \bullet \mathbf{n}^{\mathrm{C}} < 0\ , \tag{2}$$

where $\mathbf{n}^{\mathrm{R}}$ and $\mathbf{n}^{\mathrm{C}}$ are unit vectors of the outer normal to the respective boundaries of the region (Figure 2) and the symbol "$\bullet$" means the scalar product of vectors. The mass forces due to lateral density inhomogeneities in the lithosphere are neglected in this work.

In view of the aforesaid concerning the uniform orientation of the maximum compressive stress in the study region, a homogeneous field of straight trajectories of $S_{\mathrm{H,max}}$ striking at an azimuth of $\approx 325^\circ$ (Figure 2) is constructed; this value is the average strike azimuth of experimentally determined maximum compression axes (see Section 1.2). It is assumed that this field of trajectories can be extended into the western and northwestern oceanic areas of the study region $0ABC$. The Cartesian coordinate system associated with the constructed field of principal stress trajectories has its origin at the intersection point of the bounding curves $0A$ and $0B$; the x_1 axis coincides in direction with the $S_{\mathrm{H,max}}$ trajectories, and the x_2 axis is directed along trajectories of the minimum compression $S_{\mathrm{H,min}}$ (Figure 2). Evidently, the unit vectors $\mathbf{m}_1$ and $\mathbf{m}_2$ of the principal axes of the sought-for tensor $\mathbf{T}$ are spatially invariable and are directed along x_1 and x_2, respectively. Given the field of trajectories of a 2-D stress tensor, the latter can be determined by integrating equilibrium equations without invoking information on rheological properties of the lithosphere; the equilibrium equations form a closed system of hyperbolic-type differential equations with characteristics coinciding with the trajectories of principal stresses [*Mukhamediev,* 1991].

In the case of a homogeneous field of straight trajectories and vanishing horizontal mass forces, the general solution providing extreme horizontal tectonic stresses has the form

$$S_{\mathrm{H,max}} = S_{\mathrm{H,max}}(x_2),\ S_{\mathrm{H,min}} = S_{\mathrm{H,min}}(x_1)\ . \tag{3}$$

[4] When specifying the $\mathbf{t}^{\mathrm{R}}$ stress on the ridge trajectory, the ridge push is actually considered as a linear force applied at the divergent boundary. This approximation was adopted by some authors (e.g. see [*Gölke and Coblenz,* 1996; *Richardson et al.,* 1979]). Apparently, a more adequate idea is to distribute this force over a band of a finite width adjacent to MAR. In particular, *Parsons and Richter* [1980] distributed the ridge push over an oceanic lithosphere younger than 40 Ma. The ridge push specification on the MAR axis is a reasonable approximation conforming to the purposes of the present work, because the push effects are analyzed at distances much larger than the width of the aforementioned band of young oceanic lithosphere.

As seen from (3), $S_{\mathrm{H,max}}$ does not depend on x_1, and $S_{\mathrm{H,min}}$ does not depend on x_2. General solution (3) needs some comments. The integration of 3-D equilibrium equations of the medium gives [*Mukhamediev,* 1991]

$$s_{\mathrm{H,max}} = s_{\mathrm{H,max}}(x_2, x_3),\ s_{\mathrm{H,min}} = s_{\mathrm{H,min}}(x_1, x_3), \qquad s_{\mathrm{V}} = \int_0^{-x_3} \rho(x_3) g dx_3 \ . \tag{4}$$

Here, $s_{\mathrm{H,max}}$ and $s_{\mathrm{H,min}}$ are, respectively, maximum and minimum local horizontal stresses, $s_{\mathrm{V}}(x_3)$ is the vertical local principal stress, x_3 is the vertical coordinate measured upward from the Earth's surface, ρ is the density of lithosphere, and g is gravity. Formulas (4) were derived under the assumption that no lateral anomalies of density are present and with due regard to the fact that two principal stresses are nearly horizontal and their directions are virtually independent of depth in the Western Europe lithosphere (see Sections 1.1 and 1.2). Taking into account the conclusions made in [*McGarr,* 1988] concerning a hydrostatic stress state of the lithosphere in the absence of applied tectonic forces, the local stresses $s_{\mathrm{H,max}}$ and $s_{\mathrm{H,min}}$ can be represented as the superpositions

$$\begin{aligned} s_{\mathrm{H,max}} &= s^t_{\mathrm{H,max}}(x_2, x_3) + s_{\mathrm{V}}(x_3), \\ s_{\mathrm{H,min}} &= s^t_{\mathrm{H,min}}(x_2, x_3) + s_{\mathrm{V}}(x_3) \ . \end{aligned} \tag{5}$$

Here, $s^t_{\mathrm{H,max}}$ and $s^t_{\mathrm{H,min}}$ are maximum and minimum horizontal tectonic stresses. Integrating the complete local stresses over the lithosphere thickness H yields

$$\begin{aligned} \tilde{S}_{\mathrm{H,max}}(x_2) &= \frac{1}{H}\int_0^H s_{\mathrm{H,max}} dx_3 = S_{\mathrm{H,max}}(x_2) + S_{\mathrm{V}}, \\ \tilde{S}_{\mathrm{H,min}}(x_1) &= \frac{1}{H}\int_0^H s_{\mathrm{H,min}} dx_3 = S_{\mathrm{H,min}}(x_1) + S_{\mathrm{V}} \ , \end{aligned} \tag{6}$$

where

$$\begin{aligned} S_{\mathrm{H,max}}(x_2) &= \frac{1}{H}\int_0^H s^t_{\mathrm{H,max}} dx_3, \\ S_{\mathrm{H,min}}(x_2) &= \frac{1}{H}\int_0^H s^t_{\mathrm{H,min}} dx_3, \\ S_{\mathrm{V}} &= \frac{1}{H}\int_0^H s_{\mathrm{V}} dx_3 \ . \end{aligned} \tag{7}$$

Solution (3) and subsequent analysis deal with exactly tectonic stresses $S_{\mathrm{H,max}}(x_2)$ and $S_{\mathrm{H,min}}(x_1)$ averaged over the lithosphere thickness, satisfying 2-D equilibrium equations and determined by relations (7). These stresses arise in response to the action of horizontal tectonic forces and characterize the deviation of the stress state from the hydrostatic state. The above representation of stresses is possible due to the specific spatial pattern of the stress distribution in the Western Europe lithosphere, and the averaging is necessary because the boundary conditions of the problem are set just in terms of averaged tectonic stresses (see Section 5 below).

To determine the unique solution from general solution (3), one should use the boundary conditions at the western and southern boundaries of the study region, which are not characteristics (and are nowhere tangent to the latter). On specifying the distribution of the stress vector (and thereby the distribution of principal stresses) on one of these boundaries (curve $0A$ or $0C$), a solution of the Cauchy problem can be obtained in the curvilinear triangle $0AB$ or $0BC$, respectively. Then one should solve a mixed problem in the remaining triangle, with one condition (namely, the $S_{\mathrm{H,max}}$ distribution) specified on the characteristic $0B$ from the solution of the preceding Cauchy problem and with the second condition specified on the curvilinear boundary. Note that, since the curves $0A$ and $0C$ are monotonic in the coordinate system (x_1, x_2), functions and vectors defined on the boundaries $0A$ and $0C$ can be represented as a function of only one coordinate (x_1 or x_2). As required, one or another representation will be used without changing the notation of pertinent functions and vectors.

3. Solution of the Problem

I start with the solution of the Cauchy problem in $0AB$ because the push forces, unlike the collision ones, are determined more reliably (e.g. see [*Parsons and Richter,* 1980; *Richardson,* 1992]). Then, the following relation holds on $0A$ in accordance with (1):

$$p^{\mathrm{R}}\mathbf{k}^{\mathrm{R}} = -S_{\mathrm{H,max}}(\mathbf{n}^{\mathrm{R}} \cdot \mathbf{m}_1)\mathbf{m}_1 - S_{\mathrm{H,min}}(\mathbf{n}^{\mathrm{R}} \cdot \mathbf{m}_2)\mathbf{m}_2 \ . \tag{8}$$

Defining on $0A$ the directing unit vector of stresses $\mathbf{k}^{\mathrm{R}}$ as a function of x_2 (and therefore as a function of x_1) from condition (8) and using the orthogonality of the unit vectors $\mathbf{m}_1$ and $\mathbf{m}_2$, the solution of the Cauchy problem in the curvilinear triangle $0AB$ can be easily constructed. With $S_{\mathrm{H,max}}$ being independent of x_1, and $S_{\mathrm{H,min}}$, of x_2, this solution has the form

$$\begin{aligned} 0AB: \quad S_{\mathrm{H,max}}(x_2) &= -p^{\mathrm{R}} \frac{\mathbf{k}^{\mathrm{R}}(x_2) \cdot \mathbf{m}_1}{\mathbf{n}^{\mathrm{R}}(x_2) \cdot \mathbf{m}_1} \ , \\ S_{\mathrm{H,min}}(x_1) &= -p^{\mathrm{R}} \frac{\mathbf{k}^{\mathrm{R}}(x_1) \cdot \mathbf{m}_2}{\mathbf{n}^{\mathrm{R}}(x_1) \cdot \mathbf{m}_2} \ . \end{aligned} \tag{9}$$

Now I find the solution in the curvilinear triangle $0BC$. The solution obtained in $0AB$ is also valid on the characteristic $0B$ directed along the x_2 axis (Figure 2). The function

$S_{\mathrm{H,max}}(x_2)$ defined on the straight line $0B$ provides the first boundary condition for the solution of the mixed problem in $0BC$. The second condition must be set on the southern boundary, i.e. on the noncharacteristic line $0C$. Note that, before doing this, continuity of the stress vector on the characteristic $0B$ should be ensured by continuing, without any changes, the function $S_{\mathrm{H,max}}(x_2)$ defined in (9) into the region $0BC$. Thus, the magnitude of the maximum compressive stress in the entire region $0ABC$ is

$$0ABC: \quad S_{\mathrm{H,max}}(x_1,x_2) \equiv S_{\mathrm{H,max}}(x_2) - \\ -p^{\mathrm{R}}\frac{\mathbf{k}^{\mathrm{R}}(x_2)\bullet\mathbf{m}_1}{\mathbf{n}^{\mathrm{R}}(x_2)\bullet\mathbf{m}_1}\ . \tag{10}$$

this value depends solely on the MAR axis geometry and push distribution pattern along this axis and is independent of collision forces.

Based on solution (10), the stress vector on the southern boundary $0C$ can be written as

$$0C: \quad p^{\mathrm{C}}\mathbf{k}^{\mathrm{C}} = p^{\mathrm{R}}\frac{\mathbf{k}^{\mathrm{R}}\bullet\mathbf{m}_1}{\mathbf{n}^{\mathrm{R}}\bullet\mathbf{m}_1}(\mathbf{n}^{\mathrm{C}}\bullet\mathbf{m}_1)\mathbf{m}_1 - \\ -S_{\mathrm{H,min}}(\mathbf{n}^{\mathrm{C}}\bullet\mathbf{m}_2)\mathbf{m}_2\ , \tag{11}$$

hence

$$0C: \quad p^{\mathrm{C}}\mathbf{k}^{\mathrm{C}}\bullet\mathbf{m}_1 = p^{\mathrm{R}}\frac{\mathbf{k}^{\mathrm{R}}(x_2)\bullet\mathbf{m}_1}{\mathbf{n}^{\mathrm{R}}(x_2)\bullet\mathbf{m}_1}\mathbf{n}^{\mathrm{C}}(x_2)\bullet\mathbf{m}_1\ . \tag{12}$$

Relation (12) implies that, if the vector of boundary stresses $\mathbf{t}^{\mathrm{R}}$ is specified on the western boundary of the region, the projection of the collision stress vector $\mathbf{t}^{\mathrm{C}}\bullet\mathbf{m}_1$ onto the axis of the maximum compressive stress is fully determined on the southern boundary. Consequently, in order to determine $S_{\mathrm{H,min}}$ in the curvilinear triangle $0BC$, it is sufficient to specify on $0C$ either the direction $\mathbf{k}^{\mathrm{C}}$ of the stress vector $\mathbf{t}^{\mathrm{C}}$ or its modulus p^{C}.

1^*. Let the vector function $\mathbf{k}^{\mathrm{C}}(x_2)$ be given on $0C$. Then, the modulus of the stress produced by the Africa-Europe convergence is determined on the southern boundary from (12):

$$0C: \quad p^{\mathrm{C}}(x_2) = p^{\mathrm{R}}\frac{\mathbf{k}^{R}(x_2)\bullet\mathbf{m}_1}{\mathbf{n}^{\mathrm{R}}(x_2)\bullet\mathbf{m}_1}\frac{\mathbf{n}^{\mathrm{C}}(x_2)\bullet\mathbf{m}_1}{\mathbf{k}^{\mathrm{C}}(x_2)\bullet\mathbf{m}_1}\ . \tag{13}$$

In this case, the distribution of the minimum compressive stress in the region $0BC$ is found from (11):

$$0BC: \quad S_{\mathrm{H,min}}(x_1,x_2) \equiv S_{\mathrm{H,min}}(x_1) = \\ = -p^{\mathrm{C}}(x_1)\frac{\mathbf{k}^{\mathrm{C}}(x_1)\bullet\mathbf{m}_2}{\mathbf{n}^{\mathrm{C}}(x_1)\bullet\mathbf{m}_2}\ , \tag{14}$$

where the function $p^{\mathrm{C}}(x_1)$ is calculated from the function $p^{\mathrm{C}}(x_2)$ given by (12). Formulas (10) and (14) provide the solution of the mixed problem in the region $0BC$. To make the solution continuous in the entire region $0ABC$, the following condition must be satisfied:

$$S_{\mathrm{H,min}}\Big|_{x_1=+0} = S_{\mathrm{H,min}}\Big|_{x_1=-0}\ . \tag{15}$$

Based on (9) and (14), condition (15) takes the form

$$p^{\mathrm{C}}(0)\frac{\mathbf{k}^{\mathrm{C}}(0)\bullet\mathbf{m}_2}{\mathbf{n}^{\mathrm{C}}(0)\bullet\mathbf{m}_2} = p^{\mathrm{R}}\frac{\mathbf{k}^{\mathrm{R}}(0)\bullet\mathbf{m}_2}{\mathbf{n}^{\mathrm{R}}(0)\bullet\mathbf{m}_2}\ . \tag{16}$$

Using (13), this equality can be written as the condition

$$\frac{\mathbf{n}^{\mathrm{C}}(0)\bullet\mathbf{m}_1}{\mathbf{n}^{\mathrm{C}}(0)\bullet\mathbf{m}_2}\frac{\mathbf{k}^{\mathrm{C}}(0)\bullet\mathbf{m}_2}{\mathbf{k}^{\mathrm{C}}(0)\bullet\mathbf{m}_1} = \\ = \frac{\mathbf{n}^{\mathrm{R}}(0)\bullet\mathbf{m}_1}{\mathbf{n}^{\mathrm{R}}(0)\bullet\mathbf{m}_2}\frac{\mathbf{k}^{\mathrm{R}}(0)\bullet\mathbf{m}_2}{\mathbf{k}^{\mathrm{R}}(0)\bullet\mathbf{m}_1}\ , \tag{17}$$

which must be satisfied at the origin of coordinates ($x_1 = 0$, $x_2 = 0$).

The complete solution in the study region is given by formulas (9), (10) and (14) provided that condition (16) or (17) is satisfied.

2^*. Let the function $p^{\mathrm{C}}(x_1)$ be specified on $0C$. Then (12) defines the directing vector of collision stresses on the boundary $0C$:

$$0C: \ \mathbf{k}^{\mathrm{C}} = k_1^C\mathbf{m}_1 \pm \sqrt{1-\left(k_1^C\right)^2}\mathbf{m}_2, \\ \left(k_1^C(x_1) = \frac{p^{\mathrm{R}}}{p^C(x_1)}\frac{\mathbf{k}^{\mathrm{R}}(x_1)\bullet\mathbf{m}_1}{\mathbf{n}^{\mathrm{R}}(x_1)\bullet\mathbf{m}_1}\mathbf{n}^{\mathrm{C}}(x_1)\bullet\mathbf{m}_1\right)\ . \tag{18}$$

The solution of the mixed problem in $0BC$, as before, is determined by formulas (10) and (14), and the projection $\mathbf{k}^{\mathrm{C}}(x_1)\bullet\mathbf{m}_2$ of the directing unit vector of stresses onto the $S_{\mathrm{H,min}}$ axis in (14) is calculated from (18). As in the previous case, the complete solution in $0ABC$ is given by formulas (9), (10) and (14), complemented with the stress continuity condition (16) or (17).

4. Results of the Solution

Specifying the push force, actually distributed over a zone around MAR, on the MAR segment $0A$ allows one to choose, within certain limits, its direction $\mathbf{k}^{\mathrm{R}}$. For example, supposing that a linear push is orthogonal to the ridge axis (i.e. $\mathbf{k}^{\mathrm{R}} = -\mathbf{n}^{\mathrm{R}}$), (9) implies that the hydrostatic stress field in the region $0AB$ is

$$0AB: \quad S_{\mathrm{H,max}} = S_{\mathrm{H,min}} = p^{\mathrm{R}}\ . \tag{19}$$

Below, I address the case of a ridge push coinciding in direction with the maximum compressive stress:

$$\mathbf{k}^{\mathrm{R}} = \mathbf{m}_1\ . \tag{20}$$

Then, as follows from (10), the magnitude of the maximum compressive stress in the entire region $0ABC$ is determined,

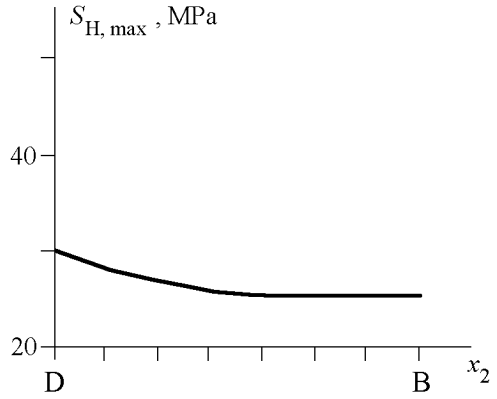

Figure 3. The $S_{\mathrm{H,max}}$ variation along the x_2 axis in the WESP region ($BB'D'D$ in Figures 1 and 2) in the case of coinciding push and $S_{\mathrm{H,max}}$ directions on the MAR axis.

irrespective of the collision forces, by the expression

$$0ABC: \quad S_{\mathrm{H,max}}(x_2) = -\frac{p^{\mathrm{R}}}{\mathbf{n}^{\mathrm{R}}(x_2)\bullet\mathbf{m}_1}\ . \qquad (21)$$

In this case, the region $0AB$ is subjected to the uniaxial compression:

$$0AB: \quad S_{\mathrm{H,min}}(x_1) = 0\ . \qquad (22)$$

The function $S_{\mathrm{H,min}}(x_1)$ in $0BC$ is determined by formula (14). In accordance with (14) and (22), the continuity of solution (15) takes the form

$$\mathbf{k}^{\mathrm{C}}(0) = -\mathbf{m}_1\ , \qquad (23)$$

and the value of collision stresses is determined from (13) and (20):

$$0C: \quad p^{\mathrm{C}}(x_2) = \frac{p^{\mathrm{R}}}{\mathbf{k}^{\mathrm{C}}(x_2)\bullet\mathbf{m}_1}\frac{\mathbf{n}^{\mathrm{C}}(x_2)\bullet\mathbf{m}_1}{\mathbf{n}^{\mathrm{R}}(x_2)\bullet\mathbf{m}_1}\ . \qquad (24)$$

The function $S_{\mathrm{H,max}}(x_2)$ in the WESP region (the rectangle $BB'D'D$ in Figures 1 and 2) is plotted in Figure 3. After *Gölke and Coblenz* [1996], I set the modulus of the stress vector on the boundary $0A$ to be $p^{\mathrm{R}} = 25$ MPa. This value is based on model push estimates (e.g. see [*Parsons and Richter,* 1980]).

The direction of the stress vector $\mathbf{t}^{\mathrm{C}}$ in the collision zone is defined as follows. Let β be the angle measured counterclockwise from the positive direction of the x_2 axis to the collision force direction $\mathbf{k}^{\mathrm{C}}$ at the southern boundary $0C$ (Figures 4a, 4b, 4c). I consider the case when the angle β is a linear function of x_2 :

$$\beta(x_2) = \frac{\pi}{2} + \frac{\partial\beta}{\partial x_2}x_2 \quad \left(\frac{\partial\beta}{\partial x_2} = \mathrm{const}\right)\ . \qquad (25)$$

Relation (25) meets stress continuity condition (23). If the gradient $\partial\beta/\partial x_2$ is negative (positive), the collision force vector $\mathbf{t}^{\mathrm{C}}$ rotates clockwise (counterclockwise), as a point on $0C$ moves from 0 to C (Figures 4a, 4c). The case $\partial\beta/\partial x_2 = 0$

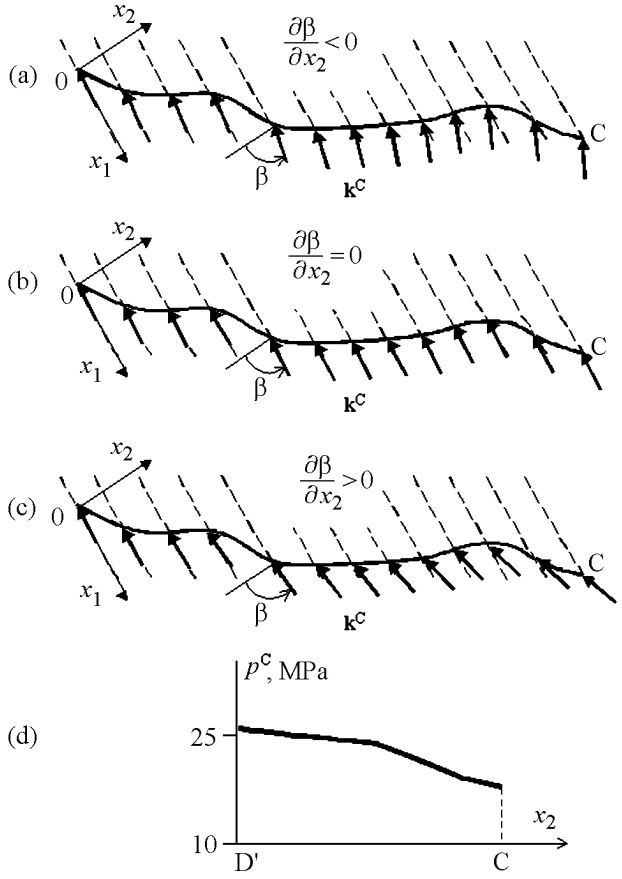

Figure 4. Distribution of the collision stress vector $\mathbf{t}^{\mathrm{C}}$ on the southern boundary $0C$ of the study region: (a) clockwise rotation of $\mathbf{t}^{\mathrm{C}}$ from 0 to C; (b) coincidence of the $\mathbf{t}^{\mathrm{C}}$ direction with the $S_{\mathrm{H,max}}$ orientation in the region; (c) counterclockwise rotation of $\mathbf{t}^{\mathrm{C}}$ from 0 to C; (d) variation of the $\mathbf{t}^{\mathrm{C}}$ stress value along $0C$.

means that the vector $\mathbf{t}^{\mathrm{C}}$ is directed along the axis of the maximum compressive stress $S_{\mathrm{H,max}}$ everywhere on $0C$.

Concrete calculations were conducted for the following three gradients of the angle β along the x_2 axis:

$$a:\ L\frac{\partial\beta}{\partial x_2} = -\frac{\pi}{18}, \quad b:\ L\frac{\partial\beta}{\partial x_2} = 0, \quad c:\ L\frac{\partial\beta}{\partial x_2} = \frac{\pi}{18}\ , \qquad (26)$$

here L is the length of $0B$. The magnitude of the collision stresses p^{C} on the segment $D'C$ of the southern boundary (Figure 2) calculated from (24) is plotted as a function of x_2 in Figure 4d. The difference between the functions $p^{\mathrm{C}}(x_2)$ calculated at different values of the gradient $\partial\beta/\partial x_2$ from (26) is too small to be reflected in Figure 4d. By contrast the stress $S_{\mathrm{H,min}}$ is much more sensitive to small variations in $\partial\beta/\partial x_2$ around zero. Figure 5 plots WESP values of the function $S_{\mathrm{H,min}}(x_1)$ calculated from (14) for three $\partial\beta/\partial x_2$ values (26). Negative values of $\partial\beta/\partial x_2$ result in positive stresses $S_{\mathrm{H,min}}$, whereas positive values of $\partial\beta/\partial x_2$ give rise to tensile stresses in the WESP region ($S_{\mathrm{H,min}} < 0$). The absolute value of $S_{\mathrm{H,min}}$ increases in the SE direction. If the

collision forces coincide in direction with $S_{\mathrm{H,max}}$ (case (b) in (26)), a uniaxial compression state ($S_{\mathrm{H,min}} = 0$) independent of the p^{C} value arises in WESP, as well as in the entire region $0ABC$. Figure 6 (a, b, c) presents the WESP stress fields corresponding to the spatial variations in $S_{\mathrm{H,max}}$ and $S_{\mathrm{H,min}}$ shown in Figures 3 and 5. The stresses $S_{\mathrm{H,max}}$ and $S_{\mathrm{H,min}}$ are shown as arrows whose length is proportional to the modulus of the respective stress. The stresses shown in Figures 6a, 6b and 6c were calculated at positive, zero and negative values of $\partial\beta/\partial x_2$, respectively.

Figure 7 presents the WESP ($BB'D'D$ in Figures 1 and 2) fields of the maximum shear stress $\tau_{\max}(x_1, x_2) = (S_{\mathrm{H,max}} - S_{\mathrm{H,min}})/2$ for three $\partial\beta/\partial x_2$ value (26).

The above results will change only insignificantly if the magnitude of collision stresses $p^{\mathrm{C}}(x_2)$ is given on the southern boundary $0C$, and their direction $\mathbf{k}^{\mathrm{C}}$ is sought for when solving the problem. In conclusion, note the replacement of the real MAR trajectory (western boundary of the study region) by the smoothed curve $0A$ (Figure 2) has also a weak effect on the model results.

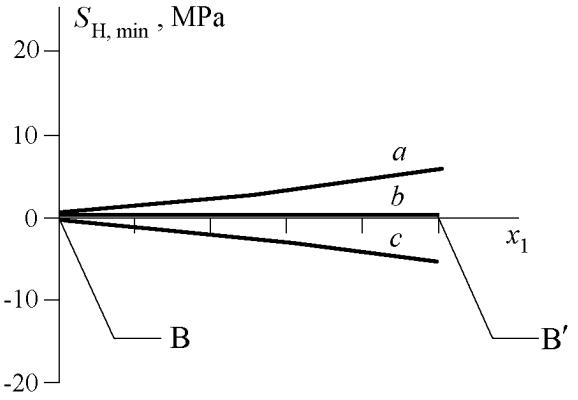

Figure 5. The $S_{\mathrm{H,min}}$ variation along the x_1 axis in the WESP area with the directions of the collision stresses $\mathbf{t}^{\mathrm{C}}$ varying linearly on the southern boundary $0C$ (see formula (25)). Curves a, b and c correspond to various directions of $\mathbf{t}^{\mathrm{C}}$ (see the respective cases in formula (26) and Figure 4).

5. Discussion of the Problem Statement and Solution Results

Now I compare the approach to the determination of tectonic stress fields proposed in this work with the approach based on traditional methods of mathematical modeling. The stress field in Western Europe was numerically modeled by *Gölke and Coblenz* [1996], who solved a plane problem of the elasticity theory with various sets of boundary conditions. The inferred solution was considered successful if model directions of $S_{\mathrm{H,max}}$ were consistent with their experimental determinations. In all of the models, displacements on the eastern boundary (which was not considered in the present work) were set at zero. In two models, zero displacements were also specified on the southern boundary (Figure 8). Collision forces were applied at the southern boundary in the other models.

Gölke and Coblenz [1996] state that the choice of boundary conditions on the eastern and southern boundaries affects only slightly the orientation and magnitude of the modeled stress $S_{\mathrm{H,max}}$. The authors themselves believe that the choice of zero displacements on the eastern boundary is unrealistic but is nevertheless justified by the fact that the model directions of $S_{\mathrm{H,max}}$ are reasonably consistent with the general tendencies of the measured stress directions. The stress state of the WESP lithosphere obtained by *Gölke and Coblenz* [1996] is close to a uniaxial one, and their resulting stress has a value of about 25 MPa and a direction close to the global NW axis of maximum compression observed in the WESP region. Thus, the results of *Gölke and Coblenz* [1996] are similar to those obtained in my work for the case of coinciding directions of the collision force $\mathbf{t}^{\mathrm{C}}$ and $S_{\mathrm{H,max}}$ axis (Figures 3, 4b, 5 (curve b) and 6b).

However, basic distinctions exist between the approaches compared:

– Gölke and Coblenz are compelled to model the eastern boundary of the region as a rigid inset, whereas my approach does not require setting boundary conditions at this boundary segment;

– in terms of the approach developed in this paper, the distribution of the collision stress vector is constrained within narrow limits by the model solution itself rather than specified on the basis of certain model considerations as is done by *Gölke and Coblenz* [1996];

– unlike the approach of these authors, in which an elastic, isotropic and mechanically homogeneous model is adopted, the present work does not use any constitutive relations at all.

These distinctions need additional comments. The classical formulation of the problem used by *Gölke and Coblenz* [1996] implies that integral constraints can only be imposed on the stresses acting along the eastern and southern boundaries of the region studied. If the push is known, the resultant vector and moment of these stresses are determined solely by the equilibrium conditions of the plate as a whole. On the contrary, the approach developed here allows one to specify the collision forces differentially, i.e. at each point of the southern boundary $0C$. Moreover, if the field of $S_{\mathrm{H,max}}$ trajectories is known throughout the region $0ABC$ (Figure 2), the constraints imposed on the collision forces $\mathbf{t}^{\mathrm{C}}(x_2)$ by equilibrium conditions, the continuity condition of solution (15), the condition $S_{\mathrm{H,min}} < S_{\mathrm{H,max}}$ and data on the spatial pattern of the stress regime are much more stringent than can seem at first glance. In particular, the vector $\mathbf{t}^{\mathrm{C}}$ can deviate only insignificantly from the $S_{\mathrm{H,max}}$ direction: if the angle β in (25) becomes much smaller than $\pi/2$, the condition $S_{\mathrm{H,min}} < S_{\mathrm{H,max}}$ is violated. Given a linear dependence of β on x_2 chosen in (26), this condition is violated (in the southeastern part of the region $0ABC$) if $\partial\beta/\partial x_2 < -\pi/9L$.

The choice of the elastic model of lithosphere allows the application of a nontraditional approach in which experimental data on the orientations of principal horizontal stresses are used as input information rather than con-

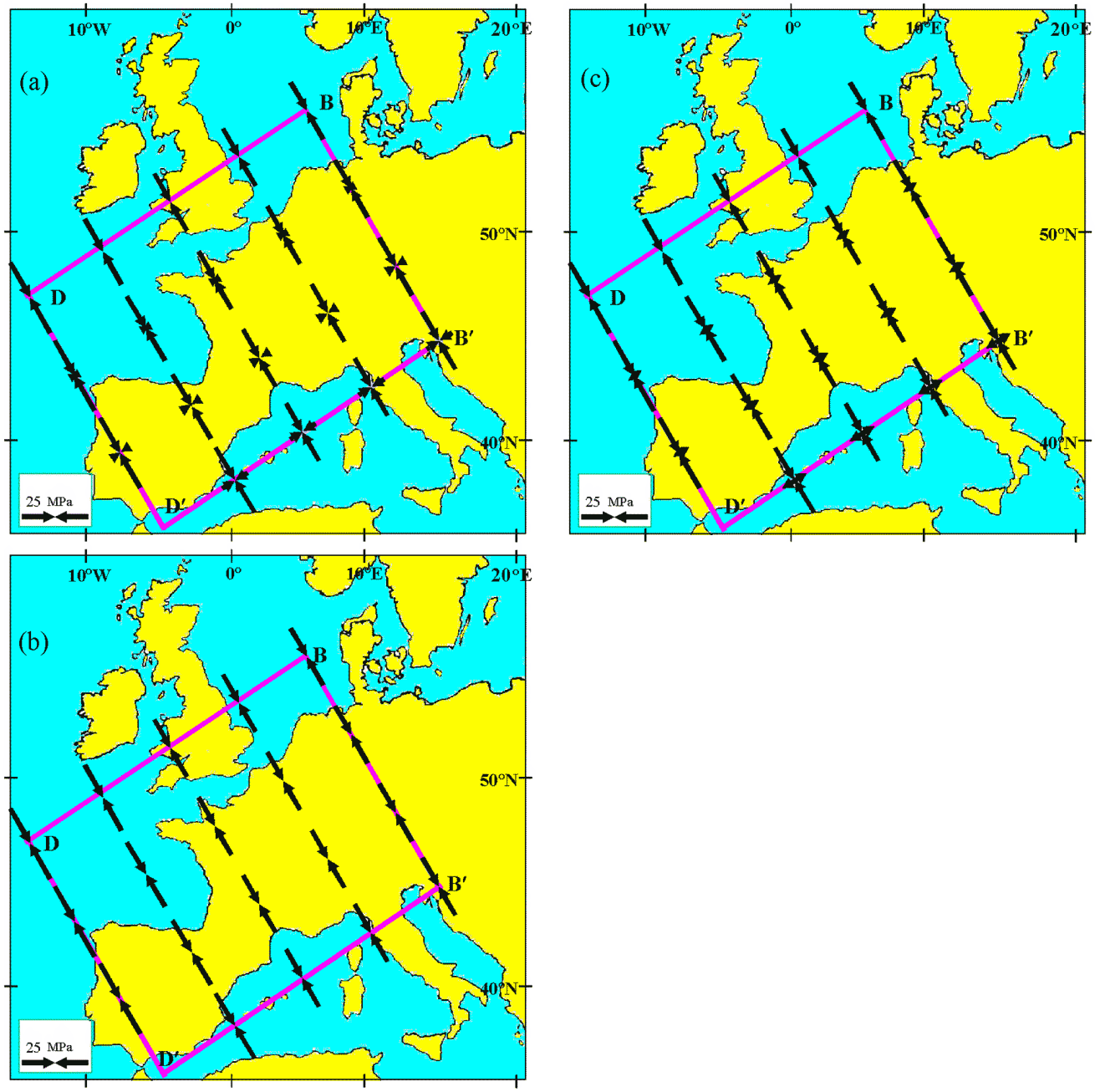

Figure 6. Global stress state of the WESP lithosphere, with push force and $S_{\mathrm{H,max}}$ stress directions coinciding on the MAR axis. The mutually orthogonal $S_{\mathrm{H,max}}$ and $S_{\mathrm{H,min}}$ stresses are shown as arrows whose length is proportional to the stress modulus. Cases a, b and c correspond to the respective curves in Figure 4 (i.e. various variants of behavior of the function $S_{\mathrm{H,min}}(x_2)$). (1) and (2) are compressive and tensile stresses, respectively.

straints on the sought-for solution as is done in [*Gölke and Coblenz,* 1996]. Data on the $S_{\mathrm{H,max}}$ orientation in the WESP region are used for constructing the field of straight trajectories, and the fields of $S_{\mathrm{H,max}}(x_1, x_2)$ and $S_{\mathrm{H,min}}(x_1, x_2)$ are determined by solving equations of the elasticity theory without invoking any evidence on boundary stresses [*Mukhamediev,* 2000; *Mukhamediev and Galybin,* 2001]. The solution for the stress field is obtained up to five arbitrary constants whose values can be defined from several instrumental measurements of stresses.

The above property of the elastic problem solution indicates that stress orientations provide relatively weak constraints on the sought-for solution. Actually, by varying the arbitrary constants and leaving the stress orientation

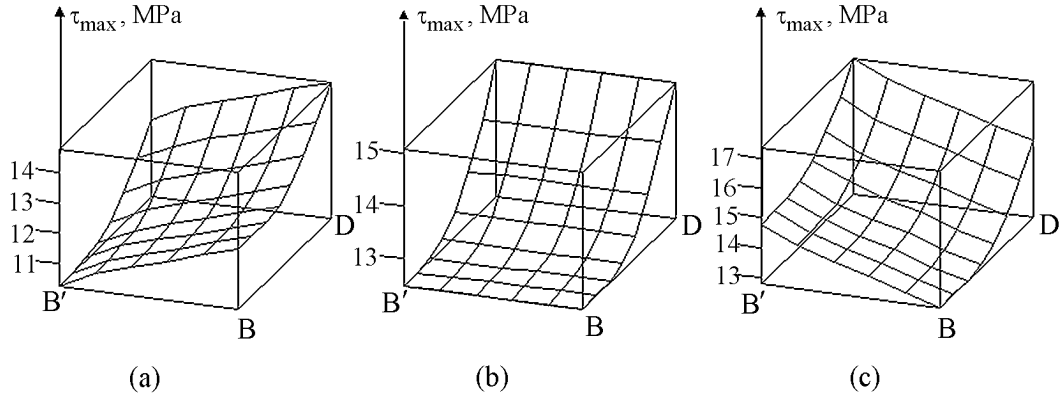

Figure 7. Distribution of the maximum shear stress in the WESP area. Surfaces a, b and c are constructed for the respective stress fields in Figure 6.

unchanged at any point, fields of $S_{\mathrm{H,max}}$ and $S_{\mathrm{H,min}}$ significantly differing both quantitatively and qualitatively can be obtained everywhere, including the boundaries of the study region [*Mukhamediev and Galybin,* 2001]. Therefore, stress fields with the same stress trajectories can be obtained with markedly different sets of boundary conditions. This property may account for the aforementioned weak dependence of the solution obtained in [*Gölke and Coblenz,* 1996] on the conditions set at the southern and eastern boundaries of Western Europe. Moreover, this by no means guarantees that at least one of the sets of boundary conditions employed in [*Gölke and Coblenz,* 1996] adequately approximates reality.

The necessity of an *a priori* choice of constitutive relations for the lithosphere material can also be regarded as a limitation of the traditional approach to the theoretical modeling of stress fields. Although an elastic model appears quite adequate for stable blocks of the lithosphere, it is not free from some internal contradictions. Using the determination of the stress state of the Western Europe as an example, these contradictions can be characterized as follows.

– First, experimental information on stress orientations is mostly gained by using seismological data on focal mechanisms, i.e. irreversible fault motions in the crust. In other words, although the lithosphere is assumed to be elastic, data on its inelastic deformations are largely invoked.

– Second, there exist spatial distributions of principal stress orientations that are inconsistent with an elastic lithosphere. Thus, if stresses of second order are taken into account, the Western Europe stress state is characterized by

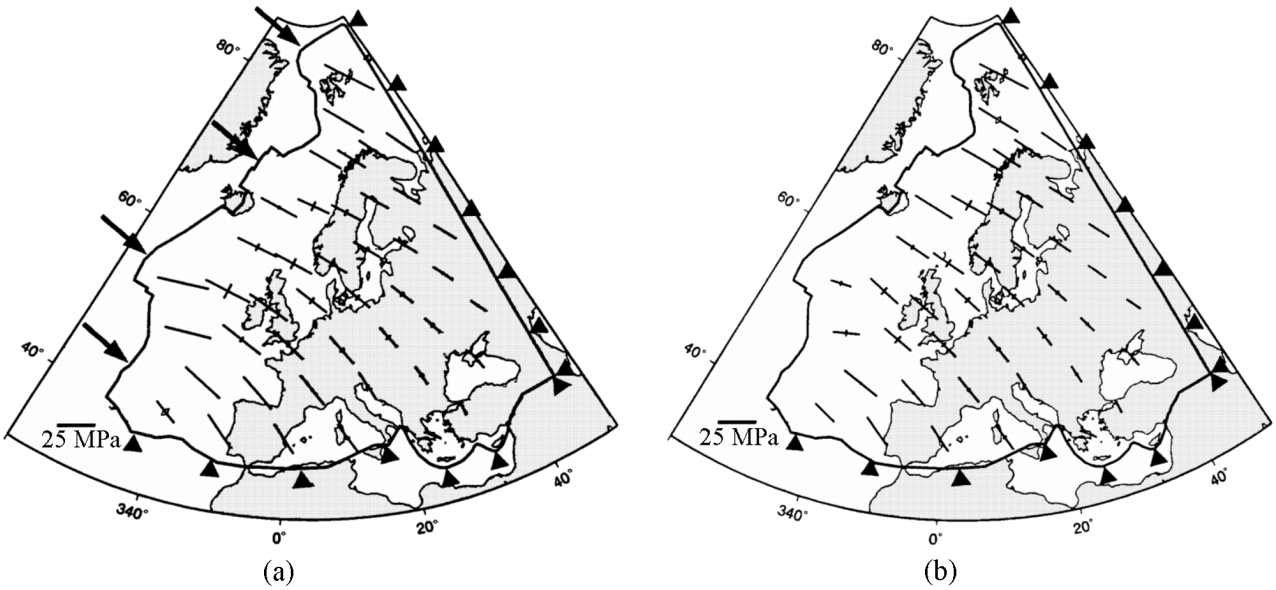

Figure 8. The $S_{\mathrm{H,max}}$ stress orientations calculated for Europe in [*Gölke and Coblenz,* 1996] from models with pinned southern and eastern boundaries: (a) the push force is applied to the ridge axis; (b) distributed push.

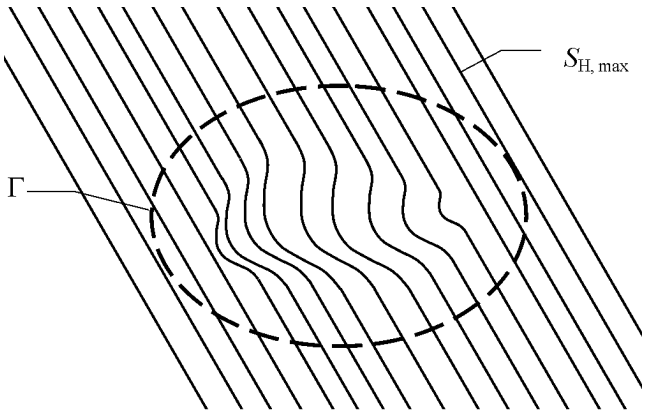

Figure 9. An example illustrating a locally disturbed field of straight trajectories of $S_{\mathrm{H,max}}$ which is inconsistent with an elastic homogeneous lithosphere. Γ is a contour encompassing the local disturbance.

a homogeneous field of straight trajectories overprinted by regional disturbances due to the presence of large geological structures such as the Alps (see Section 1.2). However, such a field of trajectories is inconsistent with a plane problem of the elasticity theory. Actually, surrounding a disturbed area by an arbitrary smooth contour Γ lying completely within the homogeneity region of the trajectories (Figure 9), one can show that the uniqueness of the solution of the elastic problem within the contour requires linearity of the trajectories [*Galybin and Mukhamediev,* 1999]. This is at variance with the assumption on the presence of a local inhomogeneity embedded in the field of straight trajectories.

The second comment implies that characteristic features of the Western Europe stress field on a regional scale cannot be obtained in terms of elastic problems irrespective of boundary conditions. In particular, no regional disturbances in the $S_{\mathrm{H,max}}$ directions are present in the solution presented by *Gölke and Coblenz* [1996] (see Figure 8). The present paper also presents a solution of the global stress field with no regional disturbances. However, as distinct from the work [*Gölke and Coblenz,* 1996], the approach developed here is basically applicable to arbitrarily structured fields of trajectories. If regional disturbances in stress trajectories are taken into account, the algorithm of solving the problem is significantly complicated as compared with that used above and should involve the solution of several hyperbolic-type boundary problems with continuity conditions imposed to link the solutions. Note also that, unlike the work [*Gölke and Coblenz,* 1996], the lithosphere can be anisotropic and mechanically inhomogeneous within the framework of the approach proposed here.

The results of the present work demonstrate the potential of this approach in determining the tectonic stress fields and reducing the arbitrariness in estimates of forces driving lithospheric plates. These results should be regarded as a first approximation to the reconstruction of real stress fields in Western Europe. Actually, they depend, to an extent, on the assumption that the field of straight trajectories of principal stresses can be extrapolated into oceanic parts of the study region $0ABC$. This simplifying assumption is not the best one because it leads to the appearance of shear stresses on the MAR trajectory. The subject of my future studies is the analysis of a model that includes, among other improvements, a weaker assumption on the pattern of trajectories in oceanic parts of the lithosphere and the examination of the stress field variation with depth. However, the main results of the present work, primarily those concerning the $S_{\mathrm{H,max}}$ field, will not change substantially. The $S_{\mathrm{H,max}}$ magnitudes are transmitted from the ridge along characteristics ($S_{\mathrm{H,max}}$ trajectories) without any significant changes, if the field of curvilinear characteristics in oceanic parts does not contain areas of their condensation and rarefaction.[5] Likewise, the model changes will not affect the validity of such a basic result as the change in sign of the $S_{\mathrm{H,min}}$ value associated with a westward or eastward deviation of the collision stress vector $\mathbf{t}^{\mathrm{C}}$ from the direction of $S_{\mathrm{H,max}}$. However, it is possible that $S_{\mathrm{H,min}}$ will not change its sign simultaneously throughout the WESP territory.

The solution presented in this paper was obtained for tectonic stresses averaged over the lithosphere thickness $H \approx$100 km. This is mainly due to the fact that the boundary stresses p^{R} refer to exactly this thickness of lithosphere. Because of the averaging of stresses, the inferred model solution cannot be directly compared with the observed depth variations of stress magnitudes and stress regime types. However, the comparison between lateral variations in the model stress field and experimental data leads to quite definite conclusions about the collision force orientation pattern and magnitudes of the related tectonic stresses. Instrumental measurements of near-surface stresses indicate that the magnitude of the minimum horizontal stress in the northern and central WESP parts is often close to zero or negative (on the order of −1 to −3 MPa) [*Becker and Davenport,* 2001; *Froidevaux et al.,* 1980]. These results indicate the tectonic stress $S_{\mathrm{H,min}}$ to be tensile, and therefore the solution presented in Figure 6c is most consistent with experimental data. It is likewise consistent with data on the spatial pattern of the stress regime, according to which the strike-slip faulting regime prevails in the WESP territory (see Section 1.2). The solution shown in Figure 6a complies with a compression regime in the WESP region. Note also that a decrease in $S_{\mathrm{H,max}}$ in the NE direction and a decrease in the negative value of $S_{\mathrm{H,min}}$ in the SE direction make the stress regime close to a tensile one in the northern Apennines region. Focal mechanisms of earthquakes in this region provide the most reliable evidence of an extension regime here (see Section 1.2). The model values of the maximum shear stress $\tau_{\max}$ in this region also reach a local extremum (Figure 7c). Thus, experimental data on the magnitude and regime of stresses indicate that the direction of the collision stresses $\mathbf{t}^{\mathrm{C}}$ is close to that of $S_{\mathrm{H,max}}$ and rotates counterclockwise when moving along the southern boundary in the eastward direction (Figure 4c).

In light of the results of this work, the discussion on the relative contributions of driving forces to the tectonic

[5]This conclusion is based on the qualitative analysis of principal stress magnitudes as a function of the distance between their trajectories [*Mukhamediev,* 1991].

stresses in the Western Europe lithosphere (see Section 1.2) can be complemented by specific considerations. Let a homogeneous system of stress orientations be known from observations, as is the case in this study. The stress magnitudes are then fully determined by the MAR push in northwestern Europe ($0AB$ in Figure 2) and by the Africa-Europe collision forces in southwestern Europe ($0BC$ in Figure 2).[6] However, the continuity of the stress field (on the line $0B$, see Figure 2) implies that the push and collision forces are coupled. Therefore, both forces equally contribute to the formation of the tectonic stress field, although the method of solving the problem described in Section 3 might induce one to believe that the push force prevails.

Both the above conclusion and the solution presented in this paper were derived under the assumption of smallness of the resultant force T_b produced by shear stresses τ_b at the base of lithosphere. There is not agreement concerning the origin of the stresses τ_b. Some researchers believe that these stresses are due to active mantle flows generally inducing the motion of continents (e.g. see [*Trubitsyn and Rykov,* 1998]). Under special assumptions on properties of the τ_b distribution over the base of lithosphere, the force T_b can significantly exceed the push [*Karakin,* 1998]. According to other concepts based on the analysis of *in situ* stress indicators, the force T_b is, on the contrary, a resistance force exerted by the underlying mantle on the lithospheric plate [*Richardson,* 1992; *Zoback,* 1992; *Zoback et al.,* 1989]. The related stresses τ_b are estimated to be small ($\leq 10^{-2}$ MPa) [*Richardson,* 1992]. When solving mathematical modeling problems of intraplate stresses, the force T_b is either neglected (e.g. see [*Gölke and Coblenz,* 1996]) or its value and direction are found from mechanical balance of forces applied to the plate under the simplifying assumption of invariability of the stress τ_b along the base of lithosphere [*Cloetingh and Wortel,* 1985; *Coblentz et al.,* 1998].

The solution obtained in Sections 3 and 4 of this paper is readily generalized to incorporate the stresses τ_b. Really, let constant shear stresses τ_b be uniformly distributed over the base of lithosphere and let they be oriented parallel to the $S_{\mathrm{H,max}}$ axis.[7] Then, given active convective flows in the mantle with the stresses τ_b directed from MAR to the collision zone, expression (10) for the stress $S_{\mathrm{H,max}}$ will contain an additional term accounting for a linear increase in $S_{\mathrm{H,\,max}}$ with increasing x_1. The magnitude of the collision stresses p^{C} will accordingly increase. On the contrary, if the underlying mantle offers a resistance to the plate motion, the stress magnitudes $S_{\mathrm{H,max}}$ in (10) experience an additional decrease that is linear in x_1 and is accompanied by a decrease in p^{C}. Note however that absolute velocities of the Eurasian plate are much smaller compared to any of the other lithospheric plates [*Gripp and Gordon,* 1990; *Richardson,* 1992]. Therefore, the approximation adopted here and consisting in vanishing stresses τ_b at the base of lithosphere is most suitable for the study of tectonic stresses in the Eurasian plate.

[6]This follows from the solution of a hyperbolic-type problem with initial data specified on a noncharacteristic line (MAR axis or collision zone trajectories.)

[7]The latter assumption is justified by the fact that the $S_{\mathrm{H,max}}$ axis is oriented along the absolute velocity direction of the plate [*Richardson,* 1992].

Conclusion

1. As is evident from experimental data, the direction of the maximum compressive stress $S_{\mathrm{H,max}}$ over the most territory of Western Europe is invariable both laterally and in depth. A uniform global NW orientation of the $S_{\mathrm{H,max}}$ axis is reflected in general characteristics of seismicity and jointing patterns of sedimentary rocks and accounts for specific features of the development of some neotectonic structures in the Western Europe lithosphere.

2. A widely accepted assumption consists in that tectonic stresses of first order in the lithosphere of the region are controlled by the push from MAR and by the collision forces in the Africa-Europe convergence zone. This assumption cannot be rigorously substantiated because data on the value and direction of the collision force are controversial. Estimation of collision forces is usually based on the Africa-Europe convergence kinematics which cannot be reliably reconstructed at present both by direct methods of satellite geodesy (due to inadequate density of the measurement network in the western and central Mediterranean) and on the basis of geological-geophysical models (due to restrictive assumptions involved in the reconstructions). However, even if a reliable kinematic reconstruction is available, the transition from movements and deformations in the collision zone to the related active forces requires additional assumptions on constitutive relations.

3. The application of traditional methods to the mathematical modeling of the stress state requires the knowledge of constitutive relations for the lithosphere material. Determination of stresses in Western Europe (as well as in other stable blocks of lithosphere) is usually based on relations of the linear elasticity theory. However, the model of a linear elastic body is basically ineffective in modeling local disturbances of the local uniform orientation of $S_{\mathrm{H,max}}$ that are produced by large geological structures such as the Alps and are typical of the stress state of the Western Europe lithosphere. This statement is based on the fact that a 2-D deformation of a homogeneous isotropic elastic body precludes local disturbances in the field of straight trajectories of principal stresses, which was proven in this work.

4. Apart from the knowledge of rheological properties of lithosphere, the traditional approach requires boundary conditions to be set on the entire perimeter of the region. In particular, this necessitates adopting hypotheses on the behavior of stresses and/or displacements on a conventional line bounding Western Europe to the east that is not an interplate boundary. Moreover, poorly constrained stresses should be specified on the southern boundary (in the collision zone). All of the aforementioned boundary conditions are chosen so as to bring into agreement the model and experimentally constrained directions of $S_{\mathrm{H,max}}$ at points where the latter have been determined. However, even the coincidence of theoretical and experimental directions of $S_{\mathrm{H,max}}$ does not guarantee the uniqueness and validity of the inferred stress field because it is still fairly sensitive to the choice of boundary stress magnitudes.

5. The direct approach developed in this paper for the determination of the field of the tectonic stress tensor uses

experimental data on the $S_{\mathrm{H,max}}$ orientation as input information. These data are employed for constructing the global field of straight trajectories of $S_{\mathrm{H,max}}$ which is extrapolated into oceanic lithosphere zones adjacent to the continental Western Europe and for solving a hyperbolic-type problem of integrating the equilibrium equations. Such a formulation of the problem does not require postulating rheological properties of the lithosphere (in particular, the lithosphere can be anisotropic and mechanically inhomogeneous). Moreover, it is not necessary to set boundary conditions on the entire perimeter of the study region: the distribution of stress vectors is only preset on a MAR axis segment ($\mathbf{t}^{\mathrm{R}}$) and in the collision zone ($\mathbf{t}^{\mathrm{C}}$).

6. The solution of the problem on tectonic stresses in Western Europe made it possible to determine the distribution of the projection of the collision stress vector $\mathbf{t}^{\mathrm{C}}$ onto the $S_{\mathrm{H,max}}$ direction at the southern boundary of the region. Certain additional conditions imposed on the solution lead to the important conclusion on the similarity between the directions of $S_{\mathrm{H,max}}$ and $\mathbf{t}^{\mathrm{C}}$ (in a long-wavelength approximation). Importantly, the restraint imposed on the collision stresses is derived directly from equilibrium conditions rather than from the kinematic analysis of the Africa-Europe convergence.

7. The model stress field in the WESP region shows that the $S_{\mathrm{H,max}}$ value decreases in the NE direction, whereas the $S_{\mathrm{H,min}}$ modulus increases in the SE direction. The spatial distribution pattern of the $S_{\mathrm{H,min}}$ value is fairly sensitive to the $\mathbf{t}^{\mathrm{C}}$ direction: the $S_{\mathrm{H,min}}$ stress is compressive, zero or tensile depending on whether the collision stress vector $\mathbf{t}^{\mathrm{C}}$ deviates westward from, coincides with or deviates eastward from the $S_{\mathrm{H,max}}$ direction. Apparently this conclusion is not critically contingent on the assumption of linearity of the principal stress trajectories in oceanic areas adjacent to Western Europe.

8. The choice of the actual direction of $\mathbf{t}^{\mathrm{C}}$ should be based on the comparison between theoretically and experimentally determined stress regimes of the Western Europe lithosphere, including instrumental measurements of stresses that provide reliable constraints on $S_{\mathrm{H,max}}$ and $S_{\mathrm{H,min}}$. Such a comparison showed that the stresses $\mathbf{t}^{\mathrm{C}}$ are close in direction to the $S_{\mathrm{H,max}}$ axis and experience a counterclockwise rotation on the southern boundary in the eastward direction. It is exactly this pattern of the collision stresses that accounts for the presence of the observed tensile stresses $S_{\mathrm{H,min}}$ and strike-slip faulting regime in most of the WESP territory.

9. The solution obtained in this work shows that the push and collision forces contribute equally to the formation of the tectonic stress field in Western Europe. The stresses at the base of lithosphere accommodating the convective flows in the mantle do not appear to have a significant effect on this field.

10. As distinct from traditional methods, the approach developed in this work is potentially promising for the modeling of second-order stresses responsible for local disturbances in the global stress field.

Acknowledgments. This work was supported in part by the Russian Foundation for Basic Research, project no. 01-05-64158.

References

Ahorner, L., Present-day stress field and seismotectonics block movements along major fault zones in western Europe, *Tectonophysics, 29,* 223–249, 1975.

Albarello, D., E. Mantovani, D. Babucci, and C. Tamburelli, Africa-Eurasia kinematics: main constraints and uncertainties, *Tectonophysics, 243,* 25–36, 1995.

Amadei, B., and O. Stephanson, *Rock stress and its measurement,* London: Chapman & Hall, 1997.

Anderson, E. M., *The dynamics of faulting and dyke formation with applications to Britain,* Edinburgh: Oliver and Boyd, 1951.

Andeweg, B., G. De Vicente, S. Cloetingh, J. Giner, and A. Muñoz Martin, Local stress fields and intraplate deformation of Iberia: variations in spatial and temporal interplay of regional stress sources, *Tectonophysics, 305,* 153–164, 1999.

Argus, D. F., R. G. Gordon, C. DeMets, and S. Stein, Closure of the Africa – Eurasia-North America plate motion circuit and tectonics of the Gloria fault, *J. Geophys. Res., 94,* (B), 5585–5602, 1989.

Balling, N., and E. Bauda, Europe's lithosphere – recent activity, in *A continent revealed, The European geotraverse,* p. 111–137, Cambridge University Press, 1992.

Becker, A., "In situ" stress data from the Jura Mountains – new results and interpretation, *Terra Nova, 11,* 9–15, 1999.

Becker, A., and C. A. Davenport, Contemporary in situ stress determination at three sites in Scotland and northern England, *J. Struct. Geol., 23,* 407–419, 2001.

Boncio, P., and G. Lavecchia, A structural model for active extension in Central Italy, *J. Geodynamics, 29,* 233–244, 2000.

Campbell, J., and A. Nothnagel, European VLBI for crustal dynamics, *J. Geodynamics, 30,* 321–326, 2000.

Cloetingh, S., and R. Wortel, Regional stress field of the Indian plate, *Geophys. Res. Lett., 12,* 77–80, 1985.

Coblentz, D. D., S. Zhou, R. R. Hillis, R. M. Richardson, and M. Sandiford, Topography, boundary forces, and the Indo-Australian intraplate stress field, *J. Geophys. Res., 103,* (B), 919–931, 1998.

Collettini, C., M. Barchi, C. Pauselli, C. Federico, and G. Pialli, Seismic expression of active extensional faults in northern Umbria (Central Italy), *J. Geodynamics, 29,* 309–321, 2000.

Cornet, F. H., and J. Yin, Analysis of induced seismicity for stress field determination and pore pressure mapping, *Pure Appl. Geophys., 145,* 677–699, 1995.

Delouis, B., H. Haessler, A. Cisternas, and L. Rivera, Stress tensor determination in France and neighbouring regions, *Tectonophysics, 221,* 413–438, 1993.

DeMets, C., R. G. Gordon, D. F. Argus, and S. Stein, Current plate motions, *Geophys. J. Int., 101,* 425–478, 1990.

De Vicente, G., G. L. Giner, A. Muñoz-Martin, J. M. Gonzáles-Casado, and R. Lindo, Determination of present-day stress tensor and neotectonic interval in the Spanish Central System and Madrid Basin, central Spain, *Tectonophysics, 266,* 405–424, 1996.

Eva, E., and S. Solarino, Variations of stress directions in the western Alpine arc, *Geophys. J. Int., 135,* 438–448, 1998.

Eva, E., S. Pastore, and N. Deichmann, Evidence for ongoing extensional deformation in the western Swiss Alps and thrust-faulting in the southwestern Alpine foreland, *J. Geodynamics, 26,* 27–47, 1998.

Frepoli, A., and A. Amato, Spatial variation in stresses in peninsular Italy and Sicily from background seismicity, *Tectonophysics, 317,* 109–124, 2000.

Froidevaux, C., C. Paquin, and M. Souriau, Tectonic stresses in France: in-situ measurements with a flat jack, *J. Geophys. Res., 85,* (B), 6349–6346, 1980.

Galybin, A. N., and Sh. A. Mukhamediev, Plane elastic boundary value problem posed on orientation of principal stresses, *J. Mech. Phys. Solids, 47,* 2381–2409, 1999.

Gapais, D., P. R. Cobbold, O. Bourgeois, D. Rouby, and M. Urreiztieta, Tectonic significance of fault slip data, *J. Struct. Geology, 22,* 881–888, 2000.

Gephart, J. W., and D. W. Forthsyth, An improved method for determining the regional stress tensor using focal mechanisms data: applications to the San Fernando earthquake sequence, *J. Geophys. Res., 89,* (B), 9305–9320, 1984.

Gölke, M., and M. Brudy, Orientation of crustal stresses in the North Sea and Barents Sea inferred from borehole breakouts, *Tectonophysics, 266,* 25–32, 1996.

Gölke, M., and D. Coblenz, Origins of the European regional stress field, *Tectonophysics, 266,* 11–24, 1996.

Gripp, A. E., and R. G. Gordon, Current plate velocities relative to hotspots incorporating the Nuvel-1 global plate motion model, *Geophys. Res. Lett., 17,* 1109–1112, 1990.

Greiner, G., In situ stress measurements in South West Germany, *Tectonophysics, 29,* 265–274, 1975.

Greiner, G., and J. H. Illies, Central Europe: active or residual stresses, *Pure Appl. Geophys., 115,* 11–26, 1977.

Grob, H., K. Kovari, and C. Amstad, Sources of error in the determination of in-situ stresses by measurements, *Tectonophysics, 29,* 29–39, 1975.

Grünthal, G., and D. Stromeyer, The recent crustal stress field in central Europe: trajectories and finite element modeling, *J. Geophys. Res., 97,* (B), 11,805–11,820, 1992.

Harper, T. R., and J. S. Szymanski, The nature and determination of stress in the accessible lithosphere, *Phil. Trans. R. Soc. London. Ser. A, 337,* 5–24, 1991.

Illies, J. H., Recent and paleo-intraplate tectonics in stable Europe and the Rhinegraben system, *Tectonophysics, 29,* 251–264, 1975.

Illies, H., and G. Greiner, Holocene movements and state of stress in the Rhinegraben rift system, *Tectonophysics, 52,* 349–359, 1979.

Kahle, H.-G., C. Straub, R. Reilinger, S. McClusky, R. King, K. Hurst, G. Veis, K. Kastens, and P. Cross, The strain rate field in the eastern Mediterranean region, estimated by repeated GPS measurements, *Tectonophysics, 294,* 237–252, 1998.

Karakin, A. V., An asymptotic decomposition technique as applied to geodynamic models of the crust and lithosphere (in Russian), *Geoinformatika, 34,* 3–6, 1998.

Letouzev J., Cenozoic paleo-stress pattern in the Alpine Foreland and structural interpretation in a platform basin, *Tectonophysics, 132,* 215–231, 1986.

McGarr, A., On the state of lithospheric stress in the absence of applied tectonic forces, *J. Geophys. Res., 93,* (B), 13,609–13,617, 1988.

Montone, P., A. Amato, and S. Pondrelli, Active stress map of Italy, *J. Geophys. Res., 104,* (B), 25,595–25,610, 1999.

Mukhamediev, Sh. A., Retrieving field of stress tensor in crustal blocks, *Izvestiya, Earth Physics, 27,* (5), 370–377, 1991.

Mukhamediev, Sh. A., Reconstruction of tectonic stresses from fault slip motions: Mathematical and physical constraints (in Russian), *Dokl. RAN, 331,* (4), 500–503, 1993.

Mukhamediev, Sh. A., Nonclassical boundary-value problems of the continuum mechanics for geodynamics, *Doklady, Earth Sciences, 373,* (5), 918–922, 2000.

Mukhamediev, Sh. A. and A. N. Galybin, A direct approach to the determination of regional stress fields: A case study of the West European, North American and Australian platforms, *Izvestia, Phys. Solid Earth, 37,* 636–652, 2001.

Müller, B., M. L. Zoback, K. Fuchs, L. Mastin, S. Gregersen, N. Pavoni, O. Stefansson, and C. Ljunggren, Regional patterns of tectonic stress in Europe, *J. Geophys. Res., 97,* (B), 11,783–11,803, 1992.

Müller, B., V. Wehrle, H. Zeyen, and K. Fuchs, Short-scale variations of tectonic regimes in the western European stress province north of the Alps and Pyrenees, *Tectonophysics, 275,* 199–219, 1997.

Noomen, R., T. A. Springer, B. A. C. Anbrosius, K. Herzberger, D. C. Kuijper, G. J. Mets, B. Overgaauw, and K. F. Wakker, Crustal deformations in the Mediterranean area computed from SLR and GPS observations, *J. Geodynamics, 21,* 73–96, 1996.

Parsons, B., and F. M. Richter, A relation between driving force and geoid anomaly associated with the mid-ocean ridges, *Earth Planet. Sci. Lett., 51,* 445–450, 1980.

Plenefisch, T., and K. P. Bonjer, The stress field in the Rhine Graben area inferred from earthquake focal mechanisms and estimation of frictional parameters, *Tectonophysics, 275,* 71–97, 1997.

Ranalli, G., Geotectonic relevance of rock-stress determinations, *Tectonophysics, 29,* 49–58, 1975.

Regenauer-Lieb, K., Plastic velocity vector diagrams applied to indentation and transpression in the Alps, *J. Geodynamics, 21,* 339–353, 1996.

Reinecker, J., and W. A. Lenhardt, Present-day stress field and deformation in eastern Austria, *Int. J. Earth Sciences, 88,* 532–550, 1999.

Richardson, R. M., Ridge forces, absolute plate motions, and the intraplate stress field, *J. Geophys. Res., 97,* (B), 11,739–11,749, 1992.

Richardson, R. M., S. C. Solomon, and N. H. Sleep, Tectonic stress in the plates, *Rev. Geophys., 17,* 981–1019, 1979.

Rivera, L., and A. Cisternas, Stress tensor and fault plane solutions for a population of earthquakes, *Bull. Seismol. Soc. Am., 80,* 600–614, 1990.

Rutqvist, J., C.-F. Tsang, and O. Stephansson, Uncertainty in the maximum principal stress estimated from hydraulic fracturing measurements due to the presence of the induced fracture, *Int. J. Rock Mech. Min. Sci., 37,* 107–120, 2000.

Savostin, L. A., J. C. Sibuet, L. P. Zonenshain, X. Le Pichon, and M. J. Roulet, Kinematic evolution of the Tethys belt from the Atlantic ocean to the Pamirs since the Triassic, *Tectonophysics, 123,* 1–35, 1986.

Scotti, O., and F. H. Cornet, In-situ stress fields and focal mechanism solutions in central France, *Geophys. Res. Lett., 21,* 2345–2348, 1994.

Trubitsyn, V. P., and V. V. Rykov, A self-consistent 2-D model of mantle convection with a floating continent, *Russian Journal of Earth Sciences, 1,* (1), 1–11, 1998.

Twiss, R. J., and J. F. Unrun, Analysis of fault slip inversions: do they constrain stress or strain rate? *J. Geophys Res. 103,* (B), 12,209–12,222, 1998.

Wirput, D., and M. Zoback, Constraining the stress tensor in the Visund field, Norwegian North Sea: Application to wellbore stability and sand production, *Int. J. Rock Mech. Min. Sci., 37,* 317–336, 2000.

Yin, J. M, and F. H. Cornet, Integrated stress determination by joint inversion of hydraulic tests and focal mechanisms, *Geophys. Res. Lett., 21,* 2645–2648, 1994.

Zoback, M. D., R. Apel, J. Baumgartner, et al., Upper-crustal strength inferred from stress measurements to 6 km depth in the KTB borehole, *Nature, 365,* 633–635, 1993.

Zoback, M. L., First- and second-order patterns of stress in the lithosphere: the world stress map project, *J. Geophys. Res., 97,* (B), 11,703–11,728, 1992.

Zoback, M. L., M. D. Zoback, J. Adams, et al., Global patterns of tectonic stress, *Nature, 341,* 291–298, 1989.

(Received 8 February, 2002)